Gaussian Beam Methods for the Schrödinger Equation in the Semi-classical Regime: Lagrangian and Eulerian Formulations *

Shi Jin[†], Hao Wu[‡], and Xu Yang[§]

September 6, 2008

Abstract

The solution to the Schrödinger equation is highly oscillatory when the rescaled Planck constant ε is small in the semiclassical regime. A direct numerical simulation requires the mesh size to be $O(\varepsilon)$. The Gaussian beam method is an efficient way to solve the high frequency wave equations asymptotically, outperforming geometric optics method in that the Gaussian beam method is accurate even at caustics.

In this paper, we solve the Schrödinger equation using both the Lagrangian and Eulerian formulations of the Gaussian beam methods. A new Eulerian Gaussian beam method is developed using the level set method based only on solving the (complex-valued) homogeneous Liouville equations. A major contribution here is that we are able to construct the Hessian matrices of the beams by using the level-set function's first derivatives. This greatly reduces the computational cost in computing the Hessian of the phase function in the Eulerian framework, yielding an Eulerian Gaussian beam method with computational complexity comparable to that of the geometric optics but with a much better accuracy around caustics.

We verify through several numerical experiments that our Gaussian beam solutions are good approximations to the Schrödinger solutions even at caustics. We also numerically study the optimal relation between the number of beams and the rescaled Planck constant ε in the Gaussian beam summation.

*This work was partially supported by NSF grant No. DMS-0608720, NSF FRG grant DMS-0757285, AFOSR grant No. FA9550-04-1-0143, NSFC Projects 10676017, the National Basic Research Program of China under the grant 2005CB321701. SJ was also supported by a Van Vleck Distinguished Research Prize from University of Wisconsin-Madison.

[†]Department of Mathematics, University of Wisconsin, Madison, WI 53706, USA (jin@math.wisc.edu)

[‡]Department of Mathematical Sciences, Tsinghua University, Beijing, 10084, China (hwu04@mails.tsinghua.edu.cn)

[§]Department of Mathematics, University of Wisconsin, Madison, WI 53706, USA (xyang@math.wisc.edu)

Key words: Schrödinger equation, Gaussian beam method, Liouville equation

1 Introduction

We are interested in the Gaussian beam methods for the numerical approximation of the Schrödinger equation:

$$i\varepsilon\frac{\partial\Psi^\varepsilon}{\partial t}+\frac{\varepsilon^2}{2}\Delta\Psi^\varepsilon-V(\boldsymbol{x})\Psi^\varepsilon=0,\quad \boldsymbol{x}\in\mathbb{R}^n\,, \tag{1.1}$$

with the WKB initial data,

$$\Psi^\varepsilon(\boldsymbol{x},0)=A_0(\boldsymbol{x})e^{iS_0(\boldsymbol{x})/\varepsilon}\,. \tag{1.2}$$

Here $\Psi^\varepsilon(\boldsymbol{x},t)$ is the wave function, ε is the re-scaled Plank constant, and $V(\boldsymbol{x})$ is the smooth potential. The physical observables can be defined in terms of $\Psi^\varepsilon(\boldsymbol{x},t)$:

$$\text{position density}\quad n^\varepsilon = |\Psi^\varepsilon|^2\,, \tag{1.3}$$

$$\text{density flux}\quad J^\varepsilon = \frac{\varepsilon}{2i}\left(\Psi^\varepsilon\nabla\overline{\Psi^\varepsilon}-\overline{\Psi^\varepsilon}\nabla\Psi^\varepsilon\right), \tag{1.4}$$

$$\text{kinetic energy}\quad E^\varepsilon = \frac{\varepsilon^2}{2}\left|\nabla\Psi^\varepsilon\right|^2. \tag{1.5}$$

The wave function $\Psi^\varepsilon(\mathbf{x},t)$ and the related physical observables become oscillatory of wave length $O(\varepsilon)$ when ε is small– in the so-called semiclassical regime. A mesh size of $O(\varepsilon)$ is required when using the time-splitting spectral method [1] to simulate (1.1)-(1.2) directly. The mesh size (and the time step as well) becomes even worse, since they need to be as small as $o(\varepsilon)$, if a finite difference method is used [21, 22]. The mesh and time step restrictions of these methods make the computation of (1.1)-(1.2) extremely expensive, especially in high dimensions.

One alternative efficient approach is to solve the equation asymptotically by the classical WKB method. Applying the ansatz

$$\Psi^\varepsilon(\boldsymbol{x},t)=A(\boldsymbol{x},t)e^{iS(\boldsymbol{x},t)/\varepsilon} \tag{1.6}$$

to (1.1), one obtains the eikonal equation for the phase $S(\boldsymbol{x},t)$ and the transport equation for the amplitude $\rho(\boldsymbol{x},t)=|A(\boldsymbol{x},t)|^2$([32]):

$$S_t+\frac{1}{2}\left|\nabla S\right|^2+V(\boldsymbol{x})=0\,, \tag{1.7}$$

$$\rho_t+\nabla\cdot(\rho\nabla S)=0\,. \tag{1.8}$$

Since the eikonal equation is of the Hamilton-Jacobi type, the solution becomes singular after caustic formation. Beyond caustics, the correct semiclassical limit of the Schrödinger equation becomes multivalued. The multivalued solution can be computed by the ray tracing methods [6, 2, 3],

wave front methods [9], moment methods [11, 14] and level set methods [16, 5, 15, 17]. We also refer the readers to the review paper on computational high frequency waves [8].

A problem with the WKB, or geometric optics based methods is that the asymptotic solution is invalid at caustics, since the amplitude $\rho(\boldsymbol{x}, t)$ blows up. None of the aforementioned methods could give accurate solutions near caustics. But on the other hand, accurately computing the solutions around the caustics is important in many applications, for example, in seismic imaging [12, 13].

The Gaussian beam method, developed for the high frequency linear waves, is an efficient approximate method that allows accurate computation of the wave amplitude around the caustics [28]. Similar to the ray tracing method, the Gaussian beam solution also has a WKB form of (1.6). The ray determined by (1.7)-(1.8) is the center of the Gaussian beam. The difference lies in that the Gaussian beam allows the phase function $S(\boldsymbol{x}, t)$ to be *complex* off its center, and the imaginary part of $S(\boldsymbol{x}, t)$ is chosen so that the solution decays exponentially away from the center. The Lagrangian formulation consists of the ray tracing equations determined by (1.7)-(1.8), which describe the trajectory of the beam center, and the Riccati equation, which describes the Hessian of the phase $S(\boldsymbol{x}, t)$. The validity of this construction at caustics is analyzed by Ralston in [29].

Lagrangian numerical methods of Gaussian beams were usually developed based on the Taylor expansion and superposition principle. The accuracy of the beam off the central ray is determined by the truncation error of Taylor expansion, and the approximate solution is given by a sum of all the beams. See [4, 13, 25]. The accuracy of the Taylor expansion was studied by Motamed and Runborg [24], and Tanushev [30] developed and analyzed higher order Gaussian beams giving better accuracy of the approximations.

Compared to the Lagrangian methods, which lose accuracy when the ray diverges and need re-interpolation to maintain the numerical accuracy which can be very complicated, the Eulerian methods based on solving PDEs on fixed grids have the advantage of a uniform accuracy. Recently, motivated by the work of Tanushev, J.L. Qian and J. Ralston [31], Leung, Qian and Burridge [19] designed an Eulerian Gaussian beam summation method for the Helmholtz equations. In their formulation, the Hessian matrix of the phase was solved by $2n^2$ *complex*-valued *inhomogeneous* Liouville equations.[1] They also introduced the semi-Lagrangian method to numerically evaluate the singular Eulerian beam summation integral.

In this paper we systematically study the Gaussian beam method for solving the Schrödinger equation in the semiclassical regime using both the

[1] After we completed this manuscript, we received the reference [18], where the Eulerian Gaussian beam method of [19] was extended to the semiclassical Schrödinger equation still using the same formulations for the Hessian of the phase as in [19].

Lagrangian and the Eulerian formulations. The Lagrangian formulation follows the classical work for linear hyperbolic equations [29]. The main contribution of this paper is a new Eulerian Gaussian beam method using the level set function. To compute the velocity and the Hessian of the phase, we only use n complex valued *homogeneous* level-set Liouville equation, rather than $2n^2$ inhomogeneous Liouville equations as in [19]. The Hessian of the phase is evaluated from the first derivatives of the level set functions. This new formulation not only significantly reduces the number of Liouville equation to be used to construct the Hessian of the phase, but also allows us to use the local level set method to further reduce the computational cost due to the homogeneity of the Liouville equations being used. As a matter of fact, the computational method for the (complex-valued) phase and amplitude is not much different from the level set method used for geometric optics computation as in [5, 16, 15]. In addition we also evaluate the Gaussian beam summation integral using the semi-Lagrangian method of [19] only near caustics, thus maintain largely the accuracy of the Eulerian method. This new method will be tested for its accuracy and efficiency by comparing with the solution of the Schrödinger equation (1.1)-(1.2).

The paper is organized as follows. In Section 2, we introduce the Lagrangian Gaussian beam formulation and summarize its properties. In Section 3, we give the detailed derivation of the new level set formulations for the Eulerian Gaussian beam method; we also discuss how to implement the summation of the Eulerian Gaussian beams, with an analysis of the computational complexity of this new method in the end. The numerical examples are given in Section 4 to test the accuracy and efficiency of the Gaussian beam methods. We make some conclusive remarks in Section 5.

2 The Lagrangian formulation

In this section, we adopt the Gaussian beam approximation to the Schrödinger equation (1.1). Let

$$\varphi_{la}^{\varepsilon}(t,\boldsymbol{x},\boldsymbol{y}_0) = A(t,\boldsymbol{y})e^{iT(t,\boldsymbol{x},\boldsymbol{y})/\varepsilon}, \tag{2.1}$$

where $\boldsymbol{y} = \boldsymbol{y}(t,\boldsymbol{y}_0)$ and $T(t,\boldsymbol{x},\boldsymbol{y})$ is given by the Taylor expansion

$$T(t,\boldsymbol{x},\boldsymbol{y}) = S(t,\boldsymbol{y})+\boldsymbol{p}(t,\boldsymbol{y})\cdot(\boldsymbol{x}-\boldsymbol{y})+\frac{1}{2}(\boldsymbol{x}-\boldsymbol{y})^\top M(t,\boldsymbol{y})(\boldsymbol{x}-\boldsymbol{y})+O(|\boldsymbol{x}-\boldsymbol{y}|^3), \tag{2.2}$$

in which $(\boldsymbol{x}-\boldsymbol{y})^\top$ is the transpose of $(\boldsymbol{x}-\boldsymbol{y})$. Here $S \in \mathbb{R}$, $\boldsymbol{p} \in \mathbb{R}^n$, $A \in \mathbb{C}$, $M \in \mathbb{C}^{n\times n}$. The imaginary part of M will be chosen so that (2.1) has a Gaussian beam profile. We call (2.1) as the beam-shaped ansatz.

The difference from the WKB ansatz is, in (2.1)-(2.2), a free parameter $\boldsymbol{y}$ is used to control the domain where the WKB analysis is applied. Actually

$\boldsymbol{y}$ plays the role of the beam center, chosen as

$$\frac{\mathrm{d}\boldsymbol{y}}{\mathrm{d}t} = \boldsymbol{p}(t,\boldsymbol{y}), \quad \boldsymbol{y}(0) = \boldsymbol{y}_0. \tag{2.3}$$

2.1 Formulation for the beam-shaped ansatz

We first derive the formulation for the beam-shaped ansatz (2.1). Plugging (2.1) into (1.1) and equating the first two leading orders of ε, one obtains the equations for T and A

$$\begin{aligned}
\frac{\partial T}{\partial t} + \frac{\partial \boldsymbol{y}}{\partial t}\cdot\nabla_{\boldsymbol{y}} T + \frac{1}{2}|\nabla_{\boldsymbol{x}} T|^2 + V &= 0, &(2.4)\\
\frac{\partial A}{\partial t} + \frac{\partial \boldsymbol{y}}{\partial t}\cdot\nabla_{\boldsymbol{y}} A + \frac{1}{2}(\triangle_{\boldsymbol{x}} T)A &= 0. &(2.5)
\end{aligned}$$

Taking the first and second derivatives with respect to $\boldsymbol{x}$ in (2.4) gives

$$\begin{aligned}
\frac{\partial(\nabla_{\boldsymbol{x}} T)}{\partial t} + \frac{\partial \boldsymbol{y}}{\partial t}\cdot\nabla_{\boldsymbol{yx}} T + \nabla_{\boldsymbol{x}} T\cdot\nabla^2_{\boldsymbol{x}} T + \nabla_{\boldsymbol{x}} V &= 0, &(2.6)\\
\frac{\partial(\nabla^2_{\boldsymbol{x}} T)}{\partial t} + \frac{\partial \boldsymbol{y}}{\partial t}\cdot\nabla_{\boldsymbol{yxx}} T + \left(\nabla^2_{\boldsymbol{x}} T\right)^2 + \nabla_{\boldsymbol{x}} T\cdot\nabla^3_{\boldsymbol{x}} T + \nabla^2_{\boldsymbol{x}} V &= 0. &(2.7)
\end{aligned}$$

Using (2.2) and evaluating (2.4)-(2.7) at $\boldsymbol{x} = \boldsymbol{y}$ yields (after ignoring the $O(|\boldsymbol{x}-\boldsymbol{y}|^3)$ term)

$$\begin{aligned}
\frac{\partial S}{\partial t} + \frac{\partial \boldsymbol{y}}{\partial t}\cdot(\nabla_{\boldsymbol{y}} S - \boldsymbol{p}) + \frac{1}{2}|\boldsymbol{p}|^2 + V &= 0, &(2.8)\\
\frac{\partial A}{\partial t} + \frac{\partial \boldsymbol{y}}{\partial t}\cdot\nabla_{\boldsymbol{y}} A + \frac{1}{2}\big(\mathrm{Tr}(M)\big)A &= 0, &(2.9)\\
\frac{\partial \boldsymbol{p}}{\partial t} + \frac{\partial \boldsymbol{y}}{\partial t}\cdot(\nabla_{\boldsymbol{y}}\boldsymbol{p} - M) + \boldsymbol{p}\cdot M + \nabla_{\boldsymbol{y}} V &= 0, &(2.10)\\
\frac{\partial M}{\partial t} + \frac{\partial \boldsymbol{y}}{\partial t}\cdot\nabla_{\boldsymbol{y}} M + M^2 + \nabla^2_{\boldsymbol{y}} V &= 0, &(2.11)
\end{aligned}$$

where $\mathrm{Tr}(M)$ is the trace of the matrix M.

Considering the $\boldsymbol{y}$-trajectory given by (2.3), then (2.8)-(2.11) can be written as a set of ODEs:

$$\begin{aligned}
\frac{\mathrm{d}\boldsymbol{y}}{\mathrm{d}t} &= \boldsymbol{p}, &(2.12)\\
\frac{\mathrm{d}\boldsymbol{p}}{\mathrm{d}t} &= -\nabla_{\boldsymbol{y}} V, &(2.13)\\
\frac{\mathrm{d}M}{\mathrm{d}t} &= -M^2 - \nabla^2_{\boldsymbol{y}} V, &(2.14)\\
\frac{\mathrm{d}S}{\mathrm{d}t} &= \frac{1}{2}|\boldsymbol{p}|^2 - V, &(2.15)\\
\frac{\mathrm{d}A}{\mathrm{d}t} &= -\frac{1}{2}\big(\mathrm{Tr}(M)\big)A. &(2.16)
\end{aligned}$$

Here $\boldsymbol{y} = \boldsymbol{y}(t, \boldsymbol{y}_0),\ \boldsymbol{p} = \boldsymbol{p}(t, \boldsymbol{y}(t, \boldsymbol{y}_0)),\ V = V(\boldsymbol{y}(t, \boldsymbol{y}_0)),\ M = M(t, \boldsymbol{y}(t, \boldsymbol{y}_0)),$ $S = S(t, \boldsymbol{y}(t, \boldsymbol{y}_0)),\ A = A(t, \boldsymbol{y}(t, \boldsymbol{y}_0))$.

The equations (2.12)-(2.16) are the Lagrangian formulation of the Gaussian beam method. (2.12)-(2.13) are called the ray-tracing equations, (2.14) is a Riccati equation for the Hessian M, which will be solved by the dynamic first order system of ray tracing equations (2.17).

We summarize some properties of these ODEs in Theorem 2.1. The results and proofs of Part 1, 2 and 3 essentially follow those in [31].

Theorem 2.1 *Let $P(t, \boldsymbol{y}(t, \boldsymbol{y}_0))$ and $R(t, \boldsymbol{y}(t, \boldsymbol{y}_0))$ be the (global) solutions of the equations*

$$\frac{\mathrm{d}P}{\mathrm{d}t} = R, \quad \frac{\mathrm{d}R}{\mathrm{d}t} = -(\nabla^2_{\boldsymbol{y}} V)P, \tag{2.17}$$

with initial conditions

$$P(0, \boldsymbol{y}_0) = I,\ R(0, \boldsymbol{y}_0) = M(0, \boldsymbol{y}_0), \tag{2.18}$$

where matrix I is the identity matrix and $Im(M(0, \boldsymbol{y}_0))$ is positive definite. Assume $M(0, \boldsymbol{y}_0)$ is symmetric, then for each initial position $\boldsymbol{y}_0$, we have the following results:

1. *$P(t, \boldsymbol{y}(t, \boldsymbol{y}_0))$ is invertible for all $t > 0$.*
2. *The solution to equation (2.14) is given by*

$$M(t, \boldsymbol{y}(t, \boldsymbol{y}_0)) = R(t, \boldsymbol{y}(t, \boldsymbol{y}_0))P^{-1}(t, \boldsymbol{y}(t, \boldsymbol{y}_0)) \tag{2.19}$$

3. *$M(t, \boldsymbol{y}(t, \boldsymbol{y}_0))$ is symmetric and $Im(M(t, \boldsymbol{y}(t, \boldsymbol{y}_0)))$ is positive definite for all $t > 0$.*
4. *Besides the Hamiltonian $V + \frac{1}{2}|\boldsymbol{p}|^2$ is conserved along the $\boldsymbol{y}$-trajectory, another quantity $A^2 \det P$ is also conserved, which means $A(t, \boldsymbol{y}(t, \boldsymbol{y}_0))$ could also be computed by*

$$A(t, \boldsymbol{y}(t, \boldsymbol{y}_0)) = \left[(\det P(t, \boldsymbol{y}(t, \boldsymbol{y}_0)))^{-1} A^2(0, \boldsymbol{y}_0)\right]^{1/2}, \tag{2.20}$$

where the square root is taken as the principle value.

Proof: Since $\boldsymbol{y}(t, \boldsymbol{y}_0)$ is not involved in the proof, we drop it for convenience and simply write $M(t, \boldsymbol{y}(t, \boldsymbol{y}_0)),\ A(t, \boldsymbol{y}(t, \boldsymbol{y}_0)),\ P(t, \boldsymbol{y}(t, \boldsymbol{y}_0))$ and $R(t, \boldsymbol{y}(t, \boldsymbol{y}_0))$ as $M(t),\ A(t),\ P(t)$ and $R(t)$ respectively.
(1) For any vector $\boldsymbol{\eta} \in \mathbb{C}^n$, by (2.17) $\boldsymbol{z}_1 = P(t)\boldsymbol{\eta}$ and $\boldsymbol{z}_2 = R(t)\boldsymbol{\eta}$ satisfy

$$\frac{\mathrm{d}\boldsymbol{z}_1}{\mathrm{d}t} = \boldsymbol{z}_2, \quad \frac{\mathrm{d}\boldsymbol{z}_2}{\mathrm{d}t} = -(\nabla^2_{\boldsymbol{y}} V)\boldsymbol{z}_1. \tag{2.21}$$

Define

$$\sigma(P,R,\boldsymbol{\eta}) = \overline{\boldsymbol{z}}_1 \cdot \boldsymbol{z}_2 - \boldsymbol{z}_1 \cdot \overline{\boldsymbol{z}}_2. \tag{2.22}$$

Note that $\nabla^2_{\boldsymbol{x}} V$ is real and symmetric, then by differentiating (2.22) with respect to t and using (2.21), one has

$$\begin{aligned}
\frac{\mathrm{d}}{\mathrm{d}t}\sigma(P,R,\boldsymbol{\eta}) &= \frac{\mathrm{d}\overline{\boldsymbol{z}}_1}{\mathrm{d}t}\cdot\boldsymbol{z}_2 + \overline{\boldsymbol{z}}_1\cdot\frac{\mathrm{d}\boldsymbol{z}_2}{\mathrm{d}t} - \frac{\mathrm{d}\boldsymbol{z}_1}{\mathrm{d}t}\cdot\overline{\boldsymbol{z}}_2 - \boldsymbol{z}_1\cdot\frac{\mathrm{d}\overline{\boldsymbol{z}}_2}{\mathrm{d}t} \\
&= \overline{\boldsymbol{z}}_2\cdot\boldsymbol{z}_2 + \overline{\boldsymbol{z}}_1\cdot\big((-\nabla^2_{\boldsymbol{y}}V)\boldsymbol{z}_1\big) - \boldsymbol{z}_2\cdot\overline{\boldsymbol{z}}_2 - \boldsymbol{z}_1\cdot\big((-\nabla^2_{\boldsymbol{x}}V)\overline{\boldsymbol{z}}_1\big) \\
&= 0.
\end{aligned}$$

Assume that $P(t)$ is singular at $t = t_0$, then there exists a non-zero vector $\boldsymbol{l} \in \mathbb{C}^n$, such that $P(t_0)\boldsymbol{l} = 0$. So we have

$$\begin{aligned}
0 &= \overline{P(t_0)\boldsymbol{l}}\cdot R(t_0)\boldsymbol{l} - P(t_0)\boldsymbol{l}\cdot\overline{R(t_0)\boldsymbol{l}} \\
&= \sigma(P(t_0),R(t_0),\boldsymbol{l}) = \sigma(P(0),R(0),\boldsymbol{l}) \\
&= \overline{P(0)\boldsymbol{l}}\cdot R(0)\boldsymbol{l} - P(0)\boldsymbol{l}\cdot\overline{R(0)\boldsymbol{l}} \\
&= \bar{\boldsymbol{l}}\cdot M(0)\boldsymbol{l} - \boldsymbol{l}\cdot\overline{M(0)\boldsymbol{l}} = 2i\bar{\boldsymbol{l}}\cdot\mathrm{Im}[M(0)]\boldsymbol{l}.
\end{aligned}$$

which is a contradiction since $\mathrm{Im}[M(0)]$ is positive definite and $\boldsymbol{l}_0$ is non-zero. In the last identity we used the symmetry of $M(0)$.

This proves the invertibility of $P(t)$.

(2) Let $M = RP^{-1}$. Using (2.17), one obtains

$$\begin{aligned}
\frac{\mathrm{d}M}{\mathrm{d}t} + M^2 + \nabla^2_{\boldsymbol{y}}V &= \frac{\mathrm{d}R}{\mathrm{d}t}P^{-1} + R\frac{\mathrm{d}P^{-1}}{\mathrm{d}t} + RP^{-1}RP^{-1} + \nabla^2_{\boldsymbol{y}}V \\
&= -(\nabla^2_{\boldsymbol{y}}V)PP^{-1} - RP^{-1}\frac{\mathrm{d}P}{\mathrm{d}t}P^{-1} + RP^{-1}RP^{-1} + \nabla^2_{\boldsymbol{y}}V \\
&= -RP^{-1}RP^{-1} + RP^{-1}RP^{-1} = 0.
\end{aligned}$$

Thus M satisfies (2.14).

(3) First, since both $M(t)$ and its transpose $M^\top(t)$ satisfy the same equation (2.14), the uniqueness (for example, Theorem 1 in [7]) implies $M(t) = M^\top(t)$ for all $t > 0$ when the initial condition $M(0)$ is symmetric.

Since we already proved that $P(t)$ is invertible, $\forall \boldsymbol{l}' \in \mathbb{C}^n$ there exist $\boldsymbol{l}$ that satisfies $\boldsymbol{l}' = P(t)\boldsymbol{l}$. Then

$$\begin{aligned}
2i\overline{\boldsymbol{l}'}\cdot\mathrm{Im}[M(t)]\boldsymbol{l}' &= 2i\overline{P(t)\boldsymbol{l}}\cdot\mathrm{Im}[M(t)]P(t)\boldsymbol{l} \\
&= \overline{P(t)\boldsymbol{l}}\cdot M(t)P(t)\boldsymbol{l} - P(t)\boldsymbol{l}\cdot\overline{M(t)P(t)\boldsymbol{l}} \\
&= \overline{P(t)\boldsymbol{l}}\cdot R(t)\boldsymbol{l} - P(t)\boldsymbol{l}\cdot\overline{R(t)\boldsymbol{l}} \\
&= \sigma(P(t),R(t),\boldsymbol{l}) = \sigma(P(0),R(0),\boldsymbol{l}) \\
&= \overline{P(0)\boldsymbol{l}}\cdot R(0)\boldsymbol{l} - P(0)\boldsymbol{l}\cdot\overline{R(0)\boldsymbol{l}} \\
&= \overline{P(0)\boldsymbol{l}}\cdot M(0)P(0)\boldsymbol{l} - P(0)\boldsymbol{l}\cdot\overline{M(0)P(0)\boldsymbol{l}} \\
&= 2i\bar{\boldsymbol{l}}\cdot\mathrm{Im}[M(0)]\boldsymbol{l}.
\end{aligned}$$

The second and last identities are got by the symmetries of $M(t)$ and $M(0)$. Because $\mathrm{Im}[M(0)]$ is positive definite, $\mathrm{Im}[M(t)]$ is also positive definite.
(4) Along the $\boldsymbol{y}$-trajectory,

$$\begin{aligned}\frac{\mathrm{d}}{\mathrm{d}t}\left(A^2\det P\right) &= 2A\frac{\mathrm{d}A}{\mathrm{d}t}\det P + A^2\frac{\mathrm{d}(\det P)}{\mathrm{d}t}\\ &= -2A\left[\frac{1}{2}\big(\mathrm{Tr}(M)\big)A\right]\det P + A^2\mathrm{Tr}\left(P^{-1}\frac{\mathrm{d}P}{\mathrm{d}t}\right)\det P\\ &= -A^2\mathrm{Tr}\left(RP^{-1}\right)\det P + A^2\mathrm{Tr}\left(P^{-1}R\right)\det P = 0.\end{aligned}$$

Hence $A^2\det P$ is conserved. □

2.2 The Lagrangian Gaussian beams summation

In this subsection, we introduce the Lagrangian Gaussian beam summation formula given by Tanushev [30]. The approximation of the WKB initial data (1.2) is shown in the next theorem.

Theorem 2.2 *Let $A_0 \in C^1(\mathbb{R}^n)\cap l^2(\mathbb{R}^n)$ and $S_0 \in C^3(\mathbb{R}^n)$, define*

$$\begin{aligned}\Psi_0^\varepsilon(\boldsymbol{x}) &= A_0(\boldsymbol{x})e^{iS_0(\boldsymbol{x})/\varepsilon},\\ \varphi_0^\varepsilon(\boldsymbol{x},\boldsymbol{y}_0) &= A_0(\boldsymbol{y}_0)e^{iT_0(\boldsymbol{x},\boldsymbol{y}_0)/\varepsilon},\end{aligned}$$

where

$$\begin{aligned}&T_0(\boldsymbol{x},\boldsymbol{y}_0) = T_{\alpha 0}(\boldsymbol{y}_0) + T_{\beta 0}\cdot(\boldsymbol{x}-\boldsymbol{y}_0) + \frac{1}{2}(\boldsymbol{x}-\boldsymbol{y}_0)^\top T_{\gamma 0}(\boldsymbol{x}-\boldsymbol{y}_0),\\ &T_{\alpha 0}(\boldsymbol{y}_0) = S_0(\boldsymbol{y}_0)\,,\quad T_{\beta 0}(\boldsymbol{y}_0) = \nabla_{\boldsymbol{x}}S_0(\boldsymbol{y}_0)\,,\quad T_{\gamma 0}(\boldsymbol{y}_0) = \nabla_{\boldsymbol{x}}^2 S_0(\boldsymbol{y}_0) + iI\,.\end{aligned}$$

Then

$$\left\|\int_{\mathbb{R}^n}\left(\frac{1}{2\pi\varepsilon}\right)^{\frac{n}{2}} r_\theta(\boldsymbol{x}-\boldsymbol{y}_0)\varphi_0^\varepsilon(\boldsymbol{x},\boldsymbol{y}_0)\mathrm{d}\boldsymbol{y}_0 - \Psi_0^\varepsilon(\boldsymbol{x})\right\|_{l^2} \le C\varepsilon^{\frac{1}{2}}.$$

where $r_\theta \in C_0^\infty(\mathbb{R}^n)$, $r_\theta \ge 0$ is a truncation function with $r_\theta \equiv 1$ in a ball of radius $\theta > 0$ about the origin and C is a constant related to θ.

By Theorem 2.2 we specify the initial data for (2.12)-(2.16) as

$$\begin{aligned}\boldsymbol{y}(0,\boldsymbol{y}_0) &= \boldsymbol{y}_0, &(2.23)\\ \boldsymbol{p}(0,\boldsymbol{y}_0) &= \nabla_{\boldsymbol{x}}S_0(\boldsymbol{y}_0), &(2.24)\\ M(0,\boldsymbol{y}_0) &= \nabla_{\boldsymbol{x}}^2 S_0(\boldsymbol{y}_0) + iI, &(2.25)\\ S(0,\boldsymbol{y}_0) &= S_0(\boldsymbol{y}_0), &(2.26)\\ A(0,\boldsymbol{y}_0) &= A_0(\boldsymbol{y}_0). &(2.27)\end{aligned}$$

Then the Gaussian beam summation solution which approximates the Schrödinger equation (1.1) is constructed as:

$$\Phi^{\varepsilon}_{la}(t,\boldsymbol{x}) = \int_{\mathbb{R}^n} \left(\frac{1}{2\pi\varepsilon}\right)^{\frac{n}{2}} r_\theta(\boldsymbol{x}-\boldsymbol{y}(t,\boldsymbol{y}_0))\varphi^{\varepsilon}_{la}(t,\boldsymbol{x},\boldsymbol{y}_0)\mathrm{d}\boldsymbol{y}_0. \tag{2.28}$$

The discrete form of (2.28) in a bounded domain is given by

$$\Phi^{\varepsilon}_{la}(t,\boldsymbol{x}) = \sum_{j=1}^{N_{\boldsymbol{y}_0}} \left(\frac{1}{2\pi\varepsilon}\right)^{\frac{n}{2}} r_\theta(\boldsymbol{x}-\boldsymbol{y}(t,\boldsymbol{y}_0^j))\varphi^{\varepsilon}_{la}(t,\boldsymbol{x},\boldsymbol{y}_0^j)\Delta\boldsymbol{y}_0, \tag{2.29}$$

where $\boldsymbol{y}_0^j$'s are the equidistant mesh points, and $N_{\boldsymbol{y}_0}$ is the number of the beams initially centered at $\boldsymbol{y}_0^j$'s.

Note that r_θ works as a cut-off function, and the cut-off error becomes large when the truncation parameter θ is taken too small. On the other hand, a big θ for wide beams makes the Taylor expansion error large. As far as we know, it is still an open question that how large the θ should be chosen when beams spread. However, for narrow beams one could take fairly large θ which makes the cut-off error almost zero. For example, a one-dimensional constant solution could be approximated by

$$1 = \int_{\mathbb{R}} \frac{1}{\sqrt{2\pi\varepsilon}} \exp\left(\frac{-(x-y_0)^2}{2\varepsilon}\right) \mathrm{d}y_0 \approx \sum_j \frac{\Delta y_0}{\sqrt{2\pi\varepsilon}} \exp\left(\frac{-(x-y_0^j)^2}{2\varepsilon}\right).$$

3 The Eulerian formulation

In the last few years, the level set method has been developed to compute the multi-valued solution of (1.7)-(1.8) which gives the correct semiclassical limit of the Schrödinger solution [16, 5, 15] *away from the caustics*. The idea is to build the velocity $\boldsymbol{u} = \nabla_{\boldsymbol{y}} S$ into the intersection of zero level sets of phase-space functions $\phi_j(t,\boldsymbol{y},\boldsymbol{\xi})$, $j = 1,\cdots,n$, i.e.

$$\phi_j(t,\boldsymbol{y},\boldsymbol{\xi}) = 0, \quad \text{at} \quad \boldsymbol{\xi} = \boldsymbol{u}(t,\boldsymbol{y}), \quad j = 1,\cdots,n. \tag{3.1}$$

If we define $\boldsymbol{\phi} = (\phi_1,\cdots,\phi_n)$, then by differentiating (3.1) with respect to $\boldsymbol{y}$ for each j, the Hessian $\nabla_{\boldsymbol{y}}\boldsymbol{u}$ satisfies

$$\nabla^2_{\boldsymbol{y}} S = \nabla_{\boldsymbol{y}}\boldsymbol{u} = -\nabla_{\boldsymbol{y}}\boldsymbol{\phi}(\nabla_{\boldsymbol{\xi}}\boldsymbol{\phi})^{-1}. \tag{3.2}$$

Comparing (3.2) with (2.19), we conjecture that

$$R = -\nabla_{\boldsymbol{y}}\boldsymbol{\phi}, \quad P = \nabla_{\boldsymbol{\xi}}\boldsymbol{\phi}. \tag{3.3}$$

Note that this conjecture does not violate the symmetry of the Hessian $\nabla_{\boldsymbol{y}}\boldsymbol{u}$ by the second and third parts of Theorem 2.1. Moreover, it also implies the divergence-free condition

$$\nabla_{\boldsymbol{\xi}} R + \nabla_{\boldsymbol{y}} P = 0. \tag{3.4}$$

which actually holds initially (2.18).

In this section, we first review the level set formulations developed in [15, 16, 19] for geometrical optics, and then prove that the conjecture (3.3) is true under an appropriate initial condition for $\boldsymbol{\phi}$. We then describe the level set algorithm for the Eulerian Gaussian beam method and the construction of the wave function for the Schrödinger equation. Although our new formulations are consistent with the Eulerian Gaussian beam method constructed in [19] for the Helmholtz equations, by making use of the observation (3.3), we introduce a much simpler and efficient numerical method than [19].

3.1 The verification of (3.3)

Define the linear Liouville operator as

$$\mathcal{L} = \partial_t + \boldsymbol{\xi} \cdot \nabla_{\boldsymbol{y}} - \nabla_{\boldsymbol{y}} V \cdot \nabla_{\boldsymbol{\xi}}.$$

As shown in [15, 16], the level set equations for the velocity, phase and amplitude are given by

$$\begin{aligned} \mathcal{L}\boldsymbol{\phi} &= 0, && (3.5)\\ \mathcal{L}S &= \frac{1}{2}|\boldsymbol{\xi}|^2 - V, && (3.6)\\ \mathcal{L}A &= \frac{1}{2}\mathrm{Tr}\left((\nabla_{\boldsymbol{\xi}}\boldsymbol{\phi})^{-1}\nabla_{\boldsymbol{y}}\boldsymbol{\phi}\right) A. && (3.7) \end{aligned}$$

If one introduces the new quantity ([15])

$$f(t, \boldsymbol{y}, \boldsymbol{\xi}) = A^2(t, \boldsymbol{y}, \boldsymbol{\xi})\det(\nabla_{\boldsymbol{\xi}}\boldsymbol{\phi}), \tag{3.8}$$

then $f(t, \boldsymbol{y}, \boldsymbol{\xi})$ satisfies the Liouville equation

$$\mathcal{L}f = 0. \tag{3.9}$$

For the Gaussian beams method in [19], two more inhomogeneous Liouville equations, which are the Eulerian formula of (2.17) for P and R, were introduced to construct the Hessian matrix

$$\begin{aligned} \mathcal{L}R &= -(\nabla_{\boldsymbol{y}}^2 V)P, && (3.10)\\ \mathcal{L}P &= R. && (3.11) \end{aligned}$$

Note that the equations (3.5)-(3.9) are *real*, while (3.10)-(3.11) are *complex* and consist of $2n^2$ equations.

By taking the gradient of the equation (3.5) with respect to $\boldsymbol{x}$ and $\boldsymbol{\xi}$ separately, we have

$$\begin{aligned} \mathcal{L}(\nabla_{\boldsymbol{y}}\boldsymbol{\phi}) &= \nabla_{\boldsymbol{y}}^2 V \nabla_{\boldsymbol{\xi}}\boldsymbol{\phi}, && (3.12)\\ \mathcal{L}(\nabla_{\boldsymbol{\xi}}\boldsymbol{\phi}) &= -\nabla_{\boldsymbol{y}}\boldsymbol{\phi}, && (3.13) \end{aligned}$$

Compare (3.10)-(3.11) with (3.12)-(3.13), we observe that $-\nabla_{\boldsymbol{y}}\boldsymbol{\phi}$ and $\nabla_{\boldsymbol{\xi}}\boldsymbol{\phi}$ satisfy the same equations as R and P. Since the Liouville equations are linear, the conjecture (3.3) is true by letting $\boldsymbol{\phi}$ be *complex* and $-\nabla_{\boldsymbol{y}}\boldsymbol{\phi}$, $\nabla_{\boldsymbol{\xi}}\boldsymbol{\phi}$ have the same initial conditions as R and P respectively.

From (2.18) and (2.25), this suggests the following initial condition for $\boldsymbol{\phi}$:

$$\boldsymbol{\phi}_0(\boldsymbol{y},\boldsymbol{\xi}) = -i\boldsymbol{y} + (\boldsymbol{\xi} - \nabla_{\boldsymbol{y}} S_0). \tag{3.14}$$

With this observation now we can solve (3.5) for *complex* $\boldsymbol{\phi}$, with initial data (3.14). Then the Hessian M is constructed by

$$M = -\nabla_{\boldsymbol{y}}\boldsymbol{\phi}(\nabla_{\boldsymbol{\xi}}\boldsymbol{\phi})^{-1} \tag{3.15}$$

where velocity $\boldsymbol{u} = -\nabla_{\boldsymbol{x}} S$ is given by the intersection of the zero-level contours of the *real* part of $\boldsymbol{\phi}$, i.e. for each component ϕ_j,

$$\mathrm{Re}[\phi_j(t,\boldsymbol{y},\boldsymbol{\xi})] = 0, \quad \text{at} \quad \boldsymbol{\xi} = \boldsymbol{u}(t,\boldsymbol{y}) = \nabla_{\boldsymbol{y}} S. \tag{3.16}$$

Note that to compute $\boldsymbol{u}, S$ and M we just need to solve n complex-valued *homogeneous* Liouville equation (3.5), while in the formulation of [19], one needs to solve n real-valued homogeneous Liouville equation (3.5) and $2n^2$ complex-valued *inhomogeneous* Liouville equations (3.10) and (3.11). Our new formulation has a computational cost only slightly higher than the level set methods for geometrical optics [15, 17]. The only difference here is that (3.5) is complex-valued while in geometrical optics computation one solves real part.

3.2 The level set algorithm

In this section, we gives the implementation details of the new level set method. We will also prove its validity at caustics.

- Step 1. Solve (3.5) for $\boldsymbol{\phi}$ *complex*, with initial condition (3.14), then obtain the velocity $\boldsymbol{u}$ by the intersection of the zero-level sets of $\mathrm{Re}\phi_j$, $j = 1, \cdots, n$.

- Step 2. Compute $-\nabla_{\boldsymbol{y}}\boldsymbol{\phi}$ and $\nabla_{\boldsymbol{\xi}}\boldsymbol{\phi}$ (note these quantities actually are already available from the first step when one discretizes the Liouville equation for $\boldsymbol{\phi}$), then the Hessian matrix is given by (3.15).

- Step 3. One can integrate the velocity $\boldsymbol{u}$ along the zero-level sets ([10, 17]) to get the phase S. The idea is to do numerical integration following each branch of the velocity. The integration constants are obtained by both the boundary condition and the fact that the multi-valued phase is continuous when it passes from one branch to the other.

For example, if we consider a bounded domain $[a, b]$ in one-dimension, the phase function is given by

$$S(t,x) = -V(a)t - \frac{1}{2}\int_0^t u^2(\tau, a)d\tau + \int_a^x u(t,s)ds + S(0,a). \quad (3.17)$$

Because $\int_a^x u(t,s)ds$ is the only term in (3.17) which affects the quadratic physical observables for fixed time t, one could take

$$S(t,x) = \int_a^x u(t,s)\mathrm{d}s \quad (3.18)$$

as the phase value in the numerical simulations of (1.3)-(1.5). For more details and in higher dimensions, see [17].

- Step 4. Solve (3.9) with the initial condition

$$f_0(\boldsymbol{y}, \boldsymbol{\xi}) = A_0^2(\boldsymbol{y}, \boldsymbol{\xi}).$$

The amplitude A is given by

$$A = (\det(\nabla_{\boldsymbol{\xi}}\boldsymbol{\phi})^{-1} f)^{1/2}, \quad (3.19)$$

in which the square root is taken as the principle value.

Remark 3.1 *All of the functions in Steps 2-4 only need to be solved locally around the zero-level sets of $Re\phi_j$, $j = 1, \cdots, n$. Namely, the entire algorithm can be implemented using the local level set methods [26, 27], thus the computational cost for mesh size Δy is $O((\Delta y)^{-n}\ln(\Delta y)^{-1})$, about the same as the local level set methods for geometrical optics computation [15, 17].*

The well-definedness of (3.15) and (3.19) is justified by the following theorem, which is the Eulerian version of Theorem 2.1.

Theorem 3.2 *Let $\boldsymbol{\phi} = \boldsymbol{\phi}(t, \boldsymbol{y}, \boldsymbol{\xi}) \in \mathbb{C}$ be the solution of (3.5) with initial data (3.14). Then we have the following: properties*

1. *$\nabla_{\boldsymbol{\xi}}\boldsymbol{\phi}$ is non-degenerate for all $t > 0$.*
2. *$Im\left(-\nabla_{\boldsymbol{y}}\boldsymbol{\phi}(\nabla_{\boldsymbol{\xi}}\boldsymbol{\phi})^{-1}\right)$ is positive definite for all $t > 0$, $\boldsymbol{y}, \boldsymbol{\xi} \in \mathbb{R}^n$.*

Proof: (1) For $\forall \boldsymbol{\eta} \in \mathbb{C}^n$, by using (3.12)-(3.13) we have

$$\begin{aligned}
& \mathcal{L}\left(\overline{(\nabla_{\boldsymbol{\xi}}\boldsymbol{\phi})\boldsymbol{\eta}} \cdot (\nabla_{\boldsymbol{y}}\boldsymbol{\phi})\boldsymbol{\eta} - (\nabla_{\boldsymbol{\xi}}\boldsymbol{\phi})\boldsymbol{\eta} \cdot \overline{(\nabla_{\boldsymbol{y}}\boldsymbol{\phi})\boldsymbol{\eta}}\right) \\
= \; & \mathcal{L}\left(\overline{(\nabla_{\boldsymbol{\xi}}\boldsymbol{\phi})\boldsymbol{\eta}}\right) \cdot (\nabla_{\boldsymbol{y}}\boldsymbol{\phi})\boldsymbol{\eta} + \overline{(\nabla_{\boldsymbol{\xi}}\boldsymbol{\phi})\boldsymbol{\eta}} \cdot \mathcal{L}\big((\nabla_{\boldsymbol{y}}\boldsymbol{\phi})\boldsymbol{\eta}\big) \\
& -\mathcal{L}\big((\nabla_{\boldsymbol{\xi}}\boldsymbol{\phi})\boldsymbol{\eta}\big) \cdot \overline{(\nabla_{\boldsymbol{y}}\boldsymbol{\phi})\boldsymbol{\eta}} - (\nabla_{\boldsymbol{\xi}}\boldsymbol{\phi})\boldsymbol{\eta} \cdot \mathcal{L}\left(\overline{(\nabla_{\boldsymbol{y}}\boldsymbol{\phi})\boldsymbol{\eta}}\right) \\
= \; & -\overline{(\nabla_{\boldsymbol{y}}\boldsymbol{\phi})\boldsymbol{\eta}} \cdot (\nabla_{\boldsymbol{y}}\boldsymbol{\phi})\boldsymbol{\eta} + \overline{(\nabla_{\boldsymbol{\xi}}\boldsymbol{\phi})\boldsymbol{\eta}} \cdot \big((\nabla_{\boldsymbol{y}}^2 V \cdot \nabla_{\boldsymbol{\xi}}\boldsymbol{\phi})\boldsymbol{\eta}\big) \\
& +(\nabla_{\boldsymbol{y}}\boldsymbol{\phi})\boldsymbol{\eta} \cdot \overline{(\nabla_{\boldsymbol{y}}\boldsymbol{\phi})\boldsymbol{\eta}} - (\nabla_{\boldsymbol{\xi}}\boldsymbol{\phi})\boldsymbol{\eta} \cdot \overline{\big((\nabla_{\boldsymbol{y}}^2 V \cdot \nabla_{\boldsymbol{\xi}}\boldsymbol{\phi})\boldsymbol{\eta}\big)} \\
= \; & 0.
\end{aligned}$$

The last equality is true because $\nabla_{\boldsymbol{y}}^2 V$ is symmetric and real.

If $\nabla_{\boldsymbol{\xi}}\boldsymbol{\phi}$ is singular at $(t_2, \boldsymbol{y}_2, \boldsymbol{\xi}_2)$, there exists a non-zero $\boldsymbol{l} \in \mathbb{C}^n$ such that $(\nabla_{\boldsymbol{\xi}}\boldsymbol{\phi})\boldsymbol{l}|_{(t_2,\boldsymbol{y}_2,\boldsymbol{\xi}_2)} = 0$. Then we have

$$\left(\overline{(\nabla_{\boldsymbol{\xi}}\boldsymbol{\phi})\boldsymbol{l}} \cdot (\nabla_{\boldsymbol{y}}\boldsymbol{\phi})\boldsymbol{l} - (\nabla_{\boldsymbol{\xi}}\boldsymbol{\phi})\boldsymbol{l} \cdot \overline{(\nabla_{\boldsymbol{y}}\boldsymbol{\phi})\boldsymbol{l}}\right)\Big|_{(t_2,\boldsymbol{y}_2,\boldsymbol{\xi}_2)} = 0.$$

Since $\mathcal{L}\left(\overline{(\nabla_{\boldsymbol{\xi}}\boldsymbol{\phi})\boldsymbol{l}} \cdot (\nabla_{\boldsymbol{y}}\boldsymbol{\phi})\boldsymbol{l} - (\nabla_{\boldsymbol{\xi}}\boldsymbol{\phi})\boldsymbol{l} \cdot \overline{(\nabla_{\boldsymbol{y}}\boldsymbol{\phi})\boldsymbol{l}}\right) = 0$, there exists $(0, \boldsymbol{y}_1, \boldsymbol{\xi}_1)$ that connects $(t_2, \boldsymbol{y}_2, \boldsymbol{\xi}_2)$ by a characteristic such that

$$\begin{aligned}
& \left(\overline{(\nabla_{\boldsymbol{\xi}}\boldsymbol{\phi})\boldsymbol{l}} \cdot (\nabla_{\boldsymbol{y}}\boldsymbol{\phi})\boldsymbol{l} - (\nabla_{\boldsymbol{\xi}}\boldsymbol{\phi})\boldsymbol{l} \cdot \overline{(\nabla_{\boldsymbol{y}}\boldsymbol{\phi})\boldsymbol{l}}\right)\Big|_{(0,\boldsymbol{y}_1,\boldsymbol{\xi}_1)} \\
= \; & \left(\overline{(\nabla_{\boldsymbol{\xi}}\boldsymbol{\phi})\boldsymbol{l}} \cdot (\nabla_{\boldsymbol{y}}\boldsymbol{\phi})\boldsymbol{l} - (\nabla_{\boldsymbol{\xi}}\boldsymbol{\phi})\boldsymbol{l} \cdot \overline{(\nabla_{\boldsymbol{y}}\boldsymbol{\phi})\boldsymbol{l}}\right)\Big|_{(t_2,\boldsymbol{y}_2,\boldsymbol{\xi}_2)} \\
= \; & 0.
\end{aligned}$$

This implies, by taking account of the initial condition (3.14),

$$-2i\bar{\boldsymbol{l}} \cdot \boldsymbol{l} = 0.$$

This is a contradiction, which proves $\nabla_{\boldsymbol{\xi}}\boldsymbol{\phi}$ is not degenerate for all $t > 0$.

(2) Since we already proved that $\nabla_{\boldsymbol{\xi}}\boldsymbol{\phi}$ is non-degenerate, $\forall \boldsymbol{l}' \in \mathbb{C}^n$ there exists an $\boldsymbol{l}$ that satisfies $\boldsymbol{l}' = (\nabla_{\boldsymbol{\xi}}\boldsymbol{\phi})\boldsymbol{l}$. Note that $-\nabla_{\boldsymbol{y}}\boldsymbol{\phi}(\nabla_{\boldsymbol{\xi}}\boldsymbol{\phi})^{-1}$ is symmetric from (3.2), then we have

$$\begin{aligned}
& 2i\overline{\boldsymbol{l}'} \cdot \mathrm{Im}\left(-\nabla_{\boldsymbol{y}}\boldsymbol{\phi}(\nabla_{\boldsymbol{\xi}}\boldsymbol{\phi})^{-1}\right)\Big|_{(t_2,\boldsymbol{y}_2,\boldsymbol{\xi}_2)} \boldsymbol{l}' \\
= \; & 2i\left(\overline{(\nabla_{\boldsymbol{\xi}}\boldsymbol{\phi})\boldsymbol{l}} \cdot \mathrm{Im}\left(-\nabla_{\boldsymbol{y}}\boldsymbol{\phi}(\nabla_{\boldsymbol{\xi}}\boldsymbol{\phi})^{-1}\right)(\nabla_{\boldsymbol{\xi}}\boldsymbol{\phi})\boldsymbol{l}\right)\Big|_{(t_2,\boldsymbol{y}_2,\boldsymbol{\xi}_2)} \\
= \; & -\left(\overline{(\nabla_{\boldsymbol{\xi}}\boldsymbol{\phi})\boldsymbol{l}} \cdot (\nabla_{\boldsymbol{y}}\boldsymbol{\phi})\boldsymbol{l} - (\nabla_{\boldsymbol{\xi}}\boldsymbol{\phi})\boldsymbol{l} \cdot \overline{(\nabla_{\boldsymbol{y}}\boldsymbol{\phi})\boldsymbol{l}}\right)\Big|_{(t_2,\boldsymbol{y}_2,\boldsymbol{\xi}_2)} \\
= \; & -\left(\overline{(\nabla_{\boldsymbol{\xi}}\boldsymbol{\phi})\boldsymbol{l}} \cdot (\nabla_{\boldsymbol{y}}\boldsymbol{\phi})\boldsymbol{l} - (\nabla_{\boldsymbol{\xi}}\boldsymbol{\phi})\boldsymbol{l} \cdot \overline{(\nabla_{\boldsymbol{y}}\boldsymbol{\phi})\boldsymbol{l}}\right)\Big|_{(0,\boldsymbol{y}_1,\boldsymbol{\xi}_1)} \\
= \; & 2i\bar{\boldsymbol{l}} \cdot \boldsymbol{l},
\end{aligned}$$

which implies that Im $\left(-\nabla_{\boldsymbol{y}}\boldsymbol{\phi}(\nabla_{\boldsymbol{\xi}}\boldsymbol{\phi})^{-1}\right)$ is positive definite. □

Remark 3.3 *Although* det $\left(Re[\nabla_{\boldsymbol{\xi}}\boldsymbol{\phi}]\right) = 0$ *at caustics, the complexified* $\boldsymbol{\phi}$ *makes* $\nabla_{\boldsymbol{\xi}}\boldsymbol{\phi}$ *non-degenerate, and the amplitude* A*, defined in (3.19), does not blow-up at caustics!*

So far we have got the phase S, the velocity $\boldsymbol{u}$, the Hessian M and the amplitude A. We show how to construct the wave function from these quantities in the next subsection.

3.3 The Eulerian Gaussian beam summation

Define

$$\varphi^{\varepsilon}_{eu}(t,\boldsymbol{x},\boldsymbol{y},\boldsymbol{\xi}) = A(t,\boldsymbol{y},\boldsymbol{\xi})e^{iT(t,\boldsymbol{x},\boldsymbol{y},\boldsymbol{\xi})/\varepsilon},$$

where

$$T(t,\boldsymbol{x},\boldsymbol{y},\boldsymbol{\xi}) = S(t,\boldsymbol{y},\boldsymbol{\xi}) + \boldsymbol{\xi}\cdot(\boldsymbol{x}-\boldsymbol{y}) + \frac{1}{2}(\boldsymbol{x}-\boldsymbol{y})^{\top}M(t,\boldsymbol{y},\boldsymbol{\xi})(\boldsymbol{x}-\boldsymbol{y}),$$

then the wave function is constructed via the following Eulerian Gaussian beam summation formula:

$$\Phi^{\varepsilon}_{eu}(t,\boldsymbol{x}) = \int_{\mathbb{R}^n}\int_{\mathbb{R}^n}\left(\frac{1}{2\pi\varepsilon}\right)^{\frac{n}{2}} r_\theta(\boldsymbol{x}-\boldsymbol{y})\varphi^{\varepsilon}_{eu}(t,\boldsymbol{x},\boldsymbol{y},\boldsymbol{\xi})\Pi_{j=1}^{n}\delta(\mathrm{Re}[\phi_j])\mathrm{d}\boldsymbol{\xi}\mathrm{d}\boldsymbol{y}, \tag{3.20}$$

in which $r_\theta \in C_0^\infty(\mathbb{R}^n)$, $r_\theta \geq 0$ is a truncation function with $r_\theta \equiv 1$ in a ball of radius $\theta > 0$ about the origin and δ is the Dirac delta function. The choice of r_θ is the same as the one in the Lagrangian formulation.

We show in the Appendix that (3.20) is consistent to the Lagrangian summation formula (2.28). (3.20) could be evaluated as a single integral about $\boldsymbol{y}$. Since the velocity becomes multivalued after caustic formation, we denote $\boldsymbol{u}_k,\ k = 1,\cdots,K$ as the velocity branches and write

$$\Phi^{\varepsilon}_{eu}(t,\boldsymbol{x}) = \int_{\mathbb{R}^n}\left(\frac{1}{2\pi\varepsilon}\right)^{\frac{n}{2}} r_\theta(\boldsymbol{x}-\boldsymbol{y})\sum_k \frac{\varphi^{\varepsilon}_{eu}(t,\boldsymbol{x},\boldsymbol{y},\boldsymbol{u}_k)}{|\det(\mathrm{Re}[\nabla_{\boldsymbol{\xi}}\boldsymbol{\phi}]_{\boldsymbol{\xi}=\boldsymbol{u}_k})|}\mathrm{d}\boldsymbol{y}, \tag{3.21}$$

Since det $\left(\mathrm{Re}[\nabla_{\boldsymbol{\xi}}\boldsymbol{\phi}]\right) = 0$ at caustics, a direct numerical integration of (3.21) loses accuracy around singularities (see Example 3 in Section 5 for the detailed numerical demonstrations). To get a better accuracy, we split (3.21) into two parts

$$I_1 = \sum_k \int_{L_1}\left(\frac{1}{2\pi\varepsilon}\right)^{\frac{n}{2}} r_\theta(\boldsymbol{x}-\boldsymbol{y})\frac{\varphi^{\varepsilon}_{eu}(t,\boldsymbol{x},\boldsymbol{y},\boldsymbol{u}_k)}{|\det(\mathrm{Re}[\nabla_{\boldsymbol{\xi}}\boldsymbol{\phi}]_{\boldsymbol{\xi}=\boldsymbol{u}_k})|}\mathrm{d}\boldsymbol{y}, \tag{3.22}$$

$$I_2 = \sum_k \int_{L_2}\left(\frac{1}{2\pi\varepsilon}\right)^{\frac{n}{2}} r_\theta(\boldsymbol{x}-\boldsymbol{y})\frac{\varphi^{\varepsilon}_{eu}(t,\boldsymbol{x},\boldsymbol{y},\boldsymbol{u}_k)}{|\det(\mathrm{Re}[\nabla_{\boldsymbol{\xi}}\boldsymbol{\phi}]_{\boldsymbol{\xi}=\boldsymbol{u}_k})|}\mathrm{d}\boldsymbol{y}, \tag{3.23}$$

where

$$L_1 = \Big\{\boldsymbol{y}\Big|\,|\det(\mathrm{Re}[\nabla_{\boldsymbol{p}}\phi](t,\boldsymbol{y},\boldsymbol{p}_j))|\geq\tau\Big\},$$
$$L_2 = \Big\{\boldsymbol{y}\Big|\,|\det(\mathrm{Re}[\nabla_{\boldsymbol{p}}\phi](t,\boldsymbol{y},\boldsymbol{p}_j))|<\tau\Big\},$$

with τ being a small parameter.

In our numerical simulations, I_1 is treated using the trapezoid quadrature rule, while the singular integral I_2 is treated by the semi-Lagrangian method introduced in [19]. For convenience we summarize the semi-Lagrangian method here. Suppose we take a number of discrete beams centered at $\boldsymbol{y}^j,\ j=1,\cdots,M_y$ with the velocity $\boldsymbol{u}_k^j$ on the contour, the idea is to trace each individual $(\boldsymbol{y}^j,\boldsymbol{u}_k^j)$ back to the initial position $(\boldsymbol{y}_0^j,\boldsymbol{u}_{k,0}^j)$ using (2.12)-(2.13) with $t\to -t$, then determine the weight function $\omega(\boldsymbol{y}_0^j)$ for it. For example in one dimension, if the two adjacent points of y_0^j are $y_0^{j_1}$ and $y_0^{j_2}$ such that $y_0^{j_1}<y_0^j<y_0^{j_2}$, then $\omega(y_0^j)=(y_0^{j_2}-y_0^{j_1})/2$ (see Page 68 in [19] for details). In this process one gets rid of the singular term by noticing that $\mathrm{d}\boldsymbol{y}_0=\dfrac{1}{|\det(\mathrm{Re}[\nabla_{\boldsymbol{\xi}}\boldsymbol{\phi}]_{\boldsymbol{\xi}=\boldsymbol{u}_k})|}\mathrm{d}\boldsymbol{y}$. The discrete form of (3.23) reads as

$$\widetilde{I_2}=\sum_{j=1}^{M_y}\sum_k\left(\frac{1}{2\pi\varepsilon}\right)^{\frac{n}{2}} r_\theta(\boldsymbol{x}-\boldsymbol{y}^j)\varphi_{eu}^\varepsilon(t,\boldsymbol{x},\boldsymbol{y}^j,\boldsymbol{u}_k^j)\omega(\boldsymbol{y}_0^j). \tag{3.24}$$

We remark here that the semi-Lagrangian method (3.24) can be used to evaluate (3.21), as was done in [19]. However, when the rays diverge backward in time, $\omega(\boldsymbol{y}_0^j)$ becomes large and one loses the accuracy of the Eulerian method. By using it only around caustics, we maintain mostly the accuracy of the Eulerian method.

3.4 Estimates on computational complexity

Since the errors of the Gaussian beam method were already discussed in [24, 30], we only focus on the analysis of the computational complexity here. There are two steps for computing the Gaussian beam solution.

1. Solving the PDEs (3.5) and (3.9) for all beams.

2. Constructing the asymptotic solution using (3.21).

The numerical cost of the first step is related to the mesh size and the time step. We will show later that the optimal mesh size is $\Delta\boldsymbol{y}=O(\varepsilon^{\frac{1}{2}})$ in the numerical simulations. We denote the numerical error of solving the PDEs as E_{num}, which introduces the error of E_{num}/ε when one constructs the wave function Φ_{eu}^ε. For this error to be minor, we require the time step taken as $\Delta t\sim\varepsilon^{\frac{1}{2}}$ in a fourth order time discretization. Then the

computational complexity of the first step is $O(\varepsilon^{-\frac{n+1}{2}} \ln \varepsilon^{-\frac{1}{2}})$ if the local level set method is used.

The numerical cost of the second step is related to the number of nodes $N_{\boldsymbol{x}}$ in the $\boldsymbol{x}$-mesh when we finally construct the solution by (3.21). To get a whole picture of the wave field, one needs to resolve the wave length, which requires $N_{\boldsymbol{x}} \sim \varepsilon^{-n}$. Due to the truncation function $r_\theta(\boldsymbol{x}-\boldsymbol{y})$ and the fact that the imaginary part of the Hessian matrix M is positive definite by Theorem 3.2, the computational cost of (3.22) is $O(1)$ for each $\boldsymbol{x}$. Since (3.23) is an integration on a small local domain (τ is small), the computational cost of (3.24) is of a smaller order compared to (3.22). So the total computational complexity of the second step is $O(\varepsilon^{-n})$.

In summary, the total computational cost is $O(\varepsilon^{-\frac{n+1}{2}} \ln \varepsilon^{-\frac{1}{2}} + \varepsilon^{-n})$. This is better than the complexity of directly solving the Schrödinger equation (1.1)-(1.2) using the Time Splitting Spectral Method [1], which is $O(\varepsilon^{-n-1} \ln \varepsilon^{-n})$.

4 The numerical examples

In this section, we present several numerical examples using both the Lagrangian and the Eulerian formulations to show the accuracy of the Gaussian beam solutions and the numerical efficiency. We compute the solution of the Schrödinger equation by the Strang Splitting Spectral Method [1]. The 'exact' Schrödinger solution Ψ^ε is got by using a very fine mesh and a very small time step with an appropriately large domain so that the periodic boundary condition does not introduce a significant error to the initial value problem. Since all the Gaussian beams are observed to be narrow in the numerical examples, the truncation parameter θ in (2.29) and (3.21) is chosen large enough so that the cut-off error is almost zero.

4.1 The Lagrangian Gaussian beam examples

We study the Lagrangian formulation numerically in this subsection. The numerical examples are chosen such that the fourth order Runger-Kutta scheme with the time step $\Delta t \sim \varepsilon^{1/2}$ is good to be used for solving (2.12)-(2.16). We analyze the asymptotic expansion error and the initial condition error in Example 1. The numerical errors of integration and ODE solvers are discussed in Example 2.

Example 1: A free particle with zero potential $V(x) = 0$. The initial conditions for the Schrödinger equation are given by

$$A_0(x) = e^{-25(x-0.5)^2},\ S_0(x) = -x^2.$$

In this example, the Gaussian beam solution (2.28) can be solved analytically

$$\Phi_{la}^{\varepsilon}(t,x)=\frac{e^{-6.25-\frac{x^2}{2\varepsilon(5t^2-4t+1)}+\frac{i}{\varepsilon}\frac{(5t-2)x^2}{2(5t^2-4t+1)}+\frac{B^2}{4A}}}{\sqrt{2A\varepsilon\big((-2+i)t+1\big)}},$$

where A and B are

$$\begin{aligned} A &= 25+\frac{(1-2t)^2}{2\varepsilon(5t^2-4t+1)}-\frac{(1-2t)t}{2\varepsilon(5t^2-4t+1)}i,\\ B &= 25+\frac{2(1-2t)x}{2\varepsilon(5t^2-4t+1)}-\frac{xt}{\varepsilon(5t^2-4t+1)}i. \end{aligned}$$

We plot the solutions at time $t=0.5$ when the caustic are generated, see Figure 1. We compare the wave amplitudes between the Gaussian beam solution $\Phi_{la}^{\varepsilon}(t,x)$ and the Schrödinger solution $\Psi^{\varepsilon}(t,x)$ for different ε's. The error comes mostly from the asymptotic expansion and the initial data approximation.

The absolute l^1, l^2 and l^∞ errors between Φ_{la}^{ε} and Ψ^{ε} for different ε's are plotted in Figure 2. One can see that the Gaussian beam solution Φ_{la}^{ε} converges in ε with an order of about 1.5 in the l^1 norm, the first order in the l^2 norm, and half order in the l^∞ norm. We gain higher order convergence rate in the l^1 and l^2 norms, because of the error cancelations in the summation of Gaussian beams (see [24, 30]).

Example 2: Consider the potential $V(x)=2x^3$, with the initial conditions

$$A_0(x)=e^{-25x^2},\ S_0(x)=\frac{1}{\pi}\cos(\pi x).$$

This example deals with a variable potential case. Since the potential $V(x)=2x^3$ makes the force *one-directional*, the wave function of (1.1)-(1.2) is *asymmetric*. Two caustics form at the time $t=0.5$.

We use a fourth order Runge-Kutta method to solve the ODE system (2.12)-(2.16) with the initial data (2.23)-(2.27) in the interval $[-1.5,1.5]$ with periodic boundary conditions. Note that the Hessian M and the amplitude A are solved via the dynamic ray tracing system (2.17), (2.19) and (2.20). In Table 1, we present the absolute l^1, l^2 and l^∞ errors between Φ^{ε} and Ψ^{ε} using different Δt's and $N_{y_0}=200$. We draw the conclusion that the numerical errors are negligible compared to the other types of errors when $\Delta t\le 0.02$ for $\varepsilon=\frac{1}{4096}$, $n=1$.

Next we study on the error coming from evaluating the integral (2.28) numerically. Evidently, the more nodes of y_0 are used, the more accurate the numerical integration will be; however, each node of y_0 corresponds to an ODE system, thus a large number of nodes will result in a high computational cost. In this example, we investigate the accuracy versus N_{y_0} for

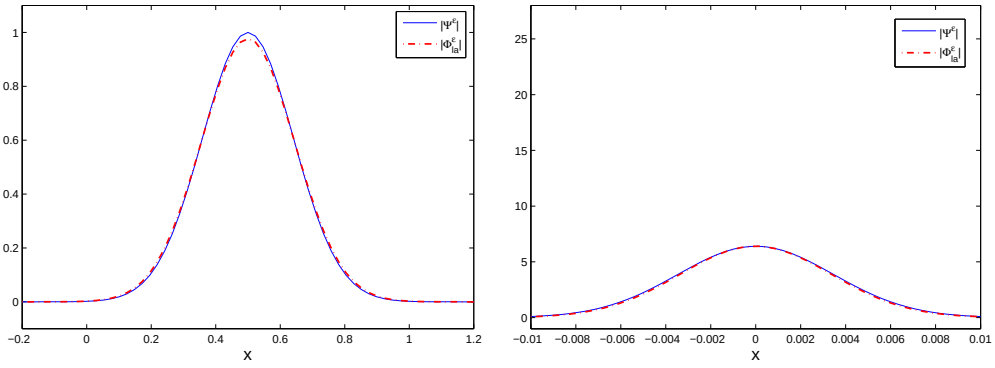

(a) $\varepsilon = \frac{1}{1024}$

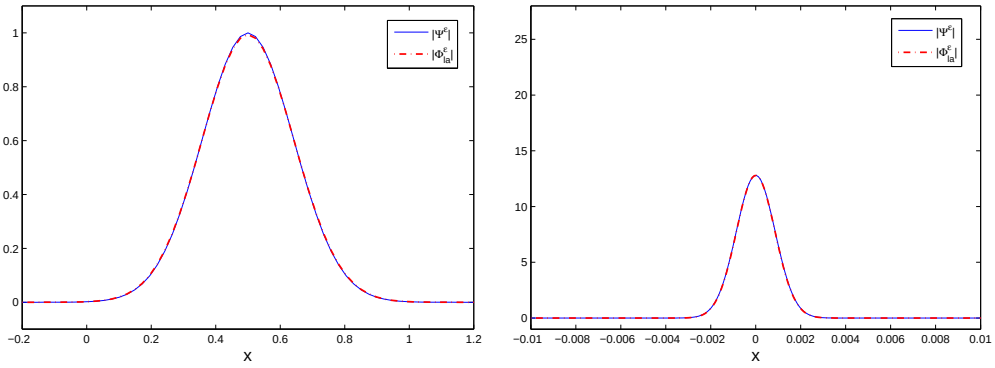

(b) $\varepsilon = \frac{1}{4096}$

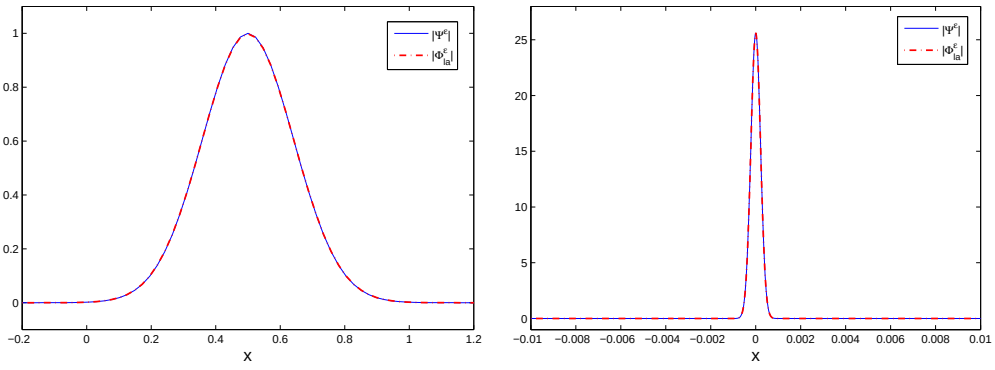

(c) $\varepsilon = \frac{1}{16384}$

Figure 1: Example 1, the Schrödinger solution $|\Psi^\varepsilon|$ versus the Gaussian beam solution $|\Phi^\varepsilon_{la}|$ at different ε's. The left figures are the comparisons at $t = 0$ (the initial time); the right figures are the comparisons at time $t = 0.5$.

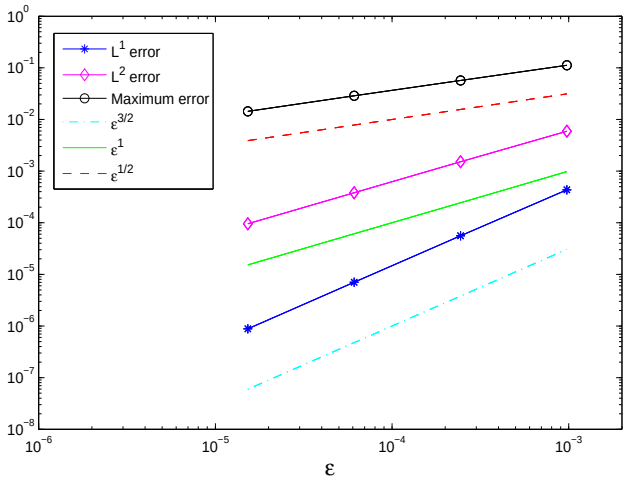

Figure 2: Example 1, the convergence rate in ε of the l^1, l^2 and l^∞ errors of the wave function.

Δt	0.04	0.02	0.01	0.005
$\|\Phi_{la}^\varepsilon - \Psi^\varepsilon\|_1$	7.88×10^{-2}	4.18×10^{-4}	4.18×10^{-4}	4.18×10^{-4}
$\|\Phi_{la}^\varepsilon - \Psi^\varepsilon\|_2$	3.51×10^{-1}	1.68×10^{-3}	1.68×10^{-3}	1.68×10^{-3}
$\|\Phi_{la}^\varepsilon - \Psi^\varepsilon\|_\infty$	2.58×10^{0}	1.24×10^{-2}	1.24×10^{-2}	1.24×10^{-2}

Table 1: the l^1, l^2 and l^∞ errors of different Δt's for Example 2.

$\varepsilon \ll 1$. We also study the optimal relation between N_{y_0} and ε which ensures a good approximation and low computational cost.

We plot the solutions at time $t = 0.5$ in Figure 3. The wave amplitudes are compared between the Schrödinger solution Ψ^ε and the Gaussian beam solution Φ^ε using different numbers of beams N_{y_0} at $\varepsilon = \frac{1}{4096}$. The absolute l^1, l^2 and l^∞ errors between Φ^ε and Ψ^ε are given in Table 2. We can see that the Gaussian beams solution converges quickly with the increasing number of beams. In Figure 4 (left), we show that $N_{y_0} \sim \varepsilon^{-\frac{1}{2}}$ is pretty much enough, and larger N_{y_0} will not reduce the error further since the other errors start to dominate.

Figure 4 (right) gives the absolute l^1, l^2 and l^∞ errors between Φ_{la}^ε and Ψ^ε for different ε's at time $t = 0.5$, where we use $N_{y_0} = 800$ and $\Delta t = 0.001$. The error convergence rate in ε is about first order in l^1 and l^2 norms, the order of 0.7894 in the l^∞ norm. We also plot the comparisons of the position density, the density flux and the kinetic energy for $\varepsilon = \frac{1}{4096}$, using $N_{y_0} = 200$, $t = 0.5$ and $\Delta t = 0.01$ in Figure 5.

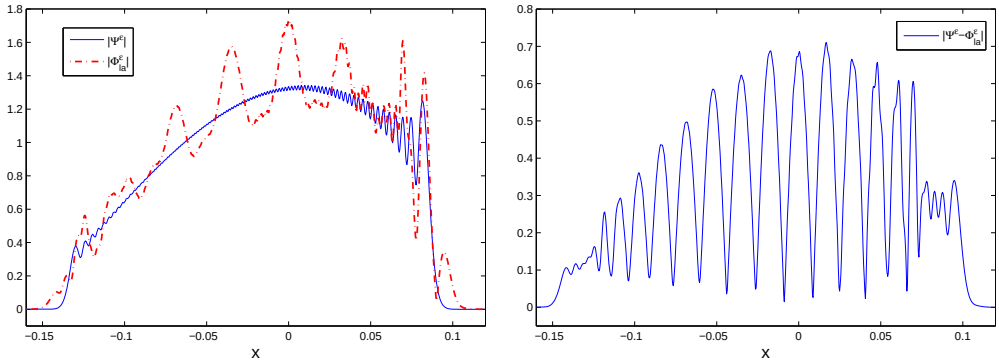

(a) $N_{y_0} = 50$

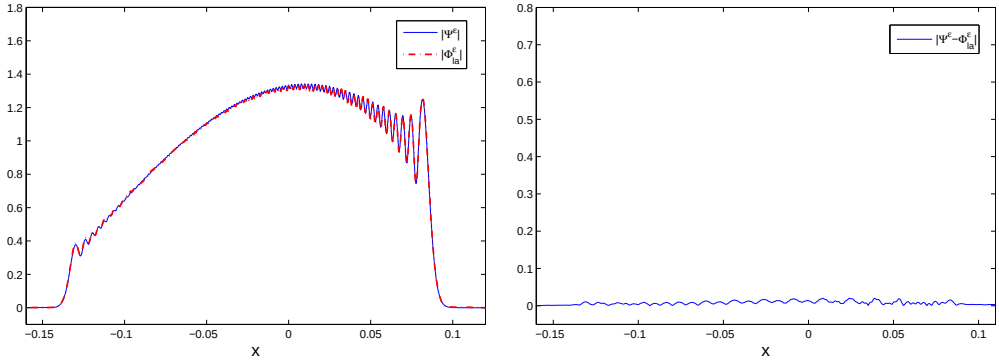

(b) $N_{y_0} = 100$

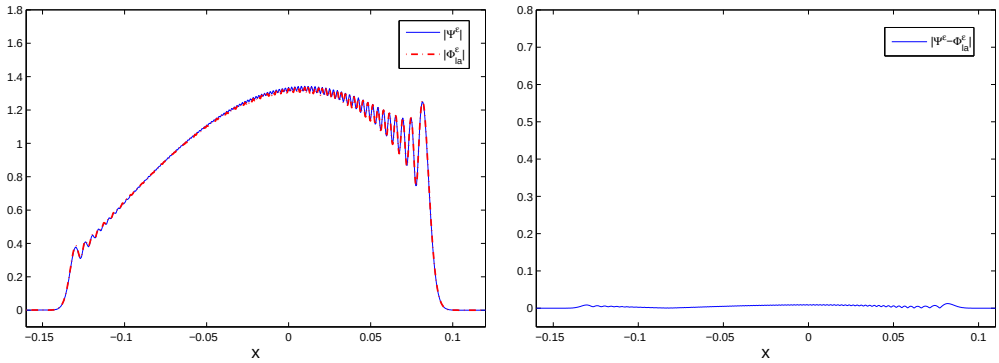

(c) $N_{y_0} = 200$

Figure 3: Example 2, the Schrödinger solution $|\Psi^\varepsilon|$ versus the Gaussian beams solution $|\Phi^\varepsilon_{la}|$ at $\varepsilon = \frac{1}{4096}$ using different N_{y_0}'s. The left figures are the comparisons at $t = 0.5$; the right figures plot the errors $|\Psi^\varepsilon - \Phi^\varepsilon_{la}|$.

N_{y_0}	50	100	150	200
$\|\Phi^\varepsilon_{la} - \Psi^\varepsilon\|_1$	2.72×10^{-2}	6.92×10^{-4}	4.18×10^{-4}	4.18×10^{-4}
$\|\Phi^\varepsilon_{la} - \Psi^\varepsilon\|_2$	1.09×10^{-1}	2.69×10^{-3}	1.68×10^{-3}	1.68×10^{-3}
$\|\Phi^\varepsilon_{la} - \Psi^\varepsilon\|_\infty$	7.10×10^{-1}	2.02×10^{-2}	1.24×10^{-2}	1.24×10^{-2}

Table 2: the l^1, l^2 and l^∞ errors at $\varepsilon = \frac{1}{4096}$ of different N_{y_0}'s for Example 2.

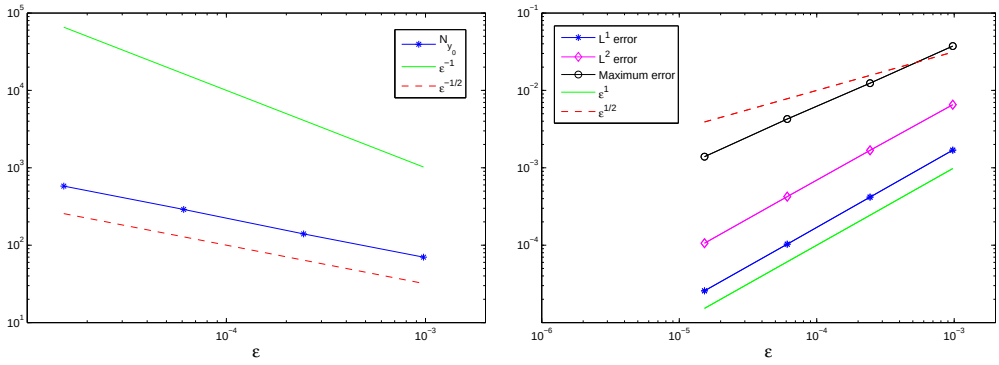

Figure 4: Example 2. Left: the plot of the optimal beam number N_{y_0} for each ε; right: the convergence rate in ε of the l^1, l^2 and l^∞ errors of the wave function.

4.2 The Eulerian Gaussian beam examples

In this subsection, we study the Gaussian beam method numerically using the Eulerian formulation. The numerical methods to the Liouville equation have been very mature by now. It could be solved by either the finite difference method [16, 17] or the semi-Lagrangian method [19, 20]. We do not address the issue of optimal Liouville solvers here.

We present two numerical examples to show the effectiveness of the Eulerian Gaussian beams method. In Example 3 (first proposed in [16]), we point out that around caustics one needs to take enough discrete beams to resolve the velocity contour well to obtain good accuracy. This is an issue not discussed in [19]. We also study a simple two-dimensional case in Example 4 which first appeared in [26].

Example 3 (1D) **:** Free motion particles with zero potential $V(x) = 0$. The initial conditions for the Schrödinger equation are given by

$$A_0(x) = e^{-25x^2}, \ S_0(x) = -\frac{1}{5}\log(2\cosh(5x)).$$

which implies that the initial density and velocity are

$$\rho_0(x) = |A_0(x)|^2 = \exp(-50x^2), \qquad u_0(x) = \partial_x S_0(x) = -\tanh(5x).$$

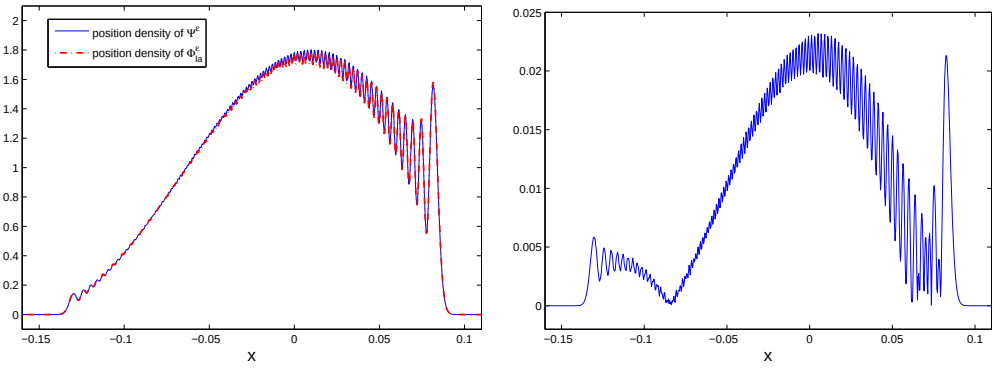

(a) The position density

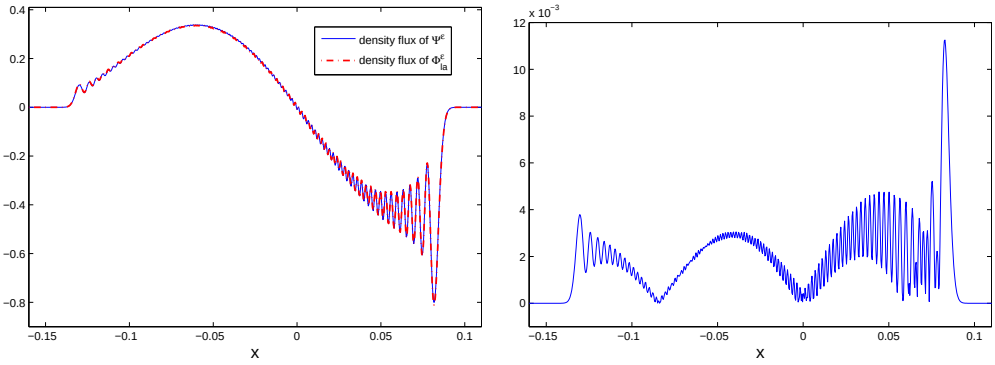

(b) The density flux

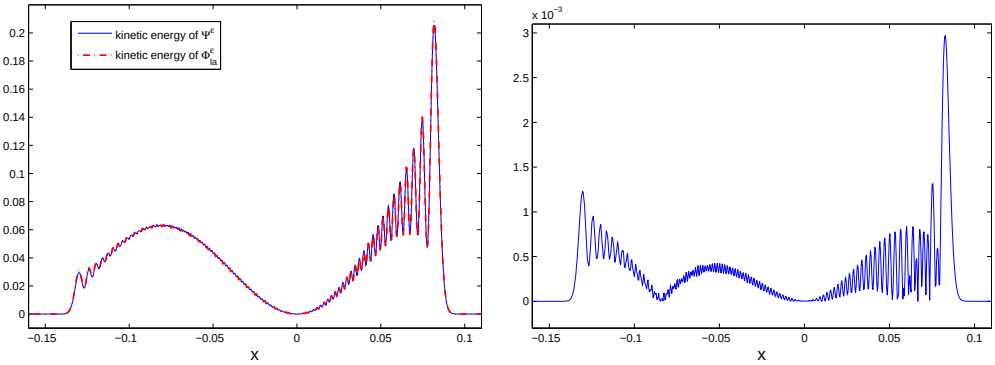

(c) The kinetic energy

Figure 5: Example 2, $\varepsilon = \frac{1}{4096}$, $N_{y_0} = 200$, $t = 0.5$ and $\Delta t = 0.01$. The left figures are the comparisons of the position density, the density flux and the kinetic energy of the Schrödinger solution Ψ^ε and the Gaussian beams solution Φ^ε_{la} at $t = 0.5$; the right figures show the errors between them.

The solutions of the Liouville equations (3.5), (3.6) and (3.9) can be solved by the characteristics method analytically:

$$\begin{aligned}
&\boldsymbol{\phi}(t,\boldsymbol{y},\boldsymbol{\xi}) = \boldsymbol{\phi}_0(\boldsymbol{y}-\boldsymbol{\xi}t,\boldsymbol{\xi}),\\
&S(t,\boldsymbol{y},\boldsymbol{\xi}) = S_0(\boldsymbol{y}-\boldsymbol{\xi}t) + tu_0^2(\boldsymbol{y}-\boldsymbol{\xi}t)/2,\\
&f(t,\boldsymbol{y},\boldsymbol{\xi}) = A_0^2(\boldsymbol{y}-\boldsymbol{\xi}t,\boldsymbol{\xi}).
\end{aligned}$$

We use $\Delta y = \Delta\xi = 0.002$ in the mesh for the Eulerian beam simulation, and take $\Delta x = \dfrac{1}{65536}$, the same mesh size as the numerical solution to the Schrödinger equation, to construct the wave function (3.21). Figure 6 shows the comparison of the wave amplitude between the Schrödinger solution Ψ^ε and the Eulerian beams solution Φ^ε_{eu} for $\varepsilon = 1\times 10^{-4}$ and at $t = 0.5$.

From the left figures of Figure 6(a)-(c), one could see that summing up the beams centered on the mesh could only approximate the Schrödinger solution accurately *away* from the caustics. In order to make good approximations *around* the caustics, one has to sum up more beams whose centers better represent the velocity contour curve. In other words, one needs to numerically resolve the singular integration (3.23) accurately by the semi-Lagrangian method. This process could be easily implemented by the Matlab subroutine 'contour'. The results are shown in the right figures of Figure 6(a)-(c). To make some comparisons we list other types of asymptotic solutions in Figure 6(d)-(f) given by geometric optics [16] and the corrected geometric optics with phase shift information (Keller-Maslov index) [17]. Since both the approximations blow up at caustics, we make some truncations when plot them. One could also notice that the Eulerian beam solution Φ^ε_{eu} naturally carries the phase shift information even when the velocity contour is not well resolved. The error of Φ^ε_{eu} is substantially smaller than Φ^ε_{GO} and Φ^ε_{PS} around the caustics.

We give the velocity contour and beams distribution around one caustic in Figure 7. This figure shows that the contour of velocity around the caustic (near $x = -0.18$) was not resolved well which causes large errors around the caustic shown in Figure 6(c) (left). Figure 8 (left) shows the amplitude convergence rates in ε are of the order of 0.9082 in the l^1 norm and the order of 0.7654 in the l^∞ norm. In Figure 8 (right), we numerically show that the optimal relationship between Δy and ε is $\Delta y \sim \varepsilon^{1/2}$ which ensures a good approximation.

Example 4 (2D)**:** Take the potential $V(x_1,x_2) = 10$ and the initial conditions of the Schrödinger equation as

$$\begin{aligned}
A_0(x_1,x_2) &= e^{-25(x_1^2+x_2^2)},\\
S_0(x_1,x_2) &= -\frac{1}{5}(\log(2\cosh(5x_1)) + \log(2\cosh(5x_2))).
\end{aligned}$$

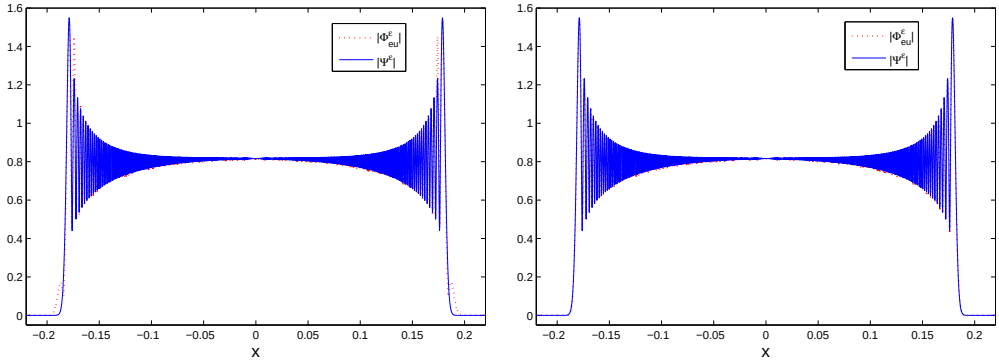

(a) Wave amplitude comparison

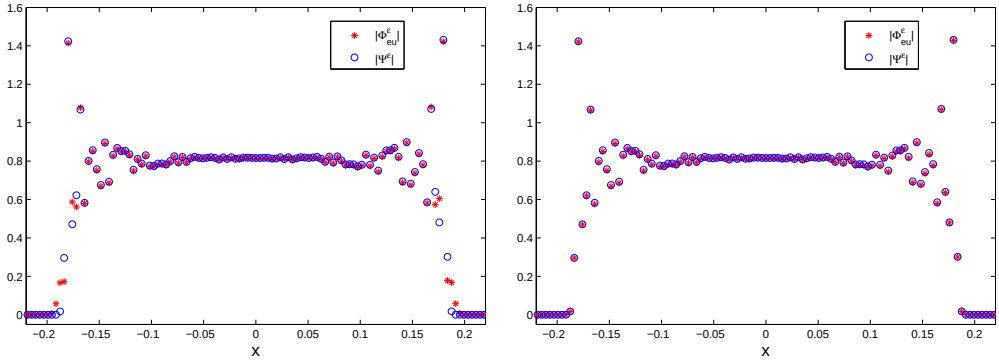

(b) Undersampled wave amplitude Comparison

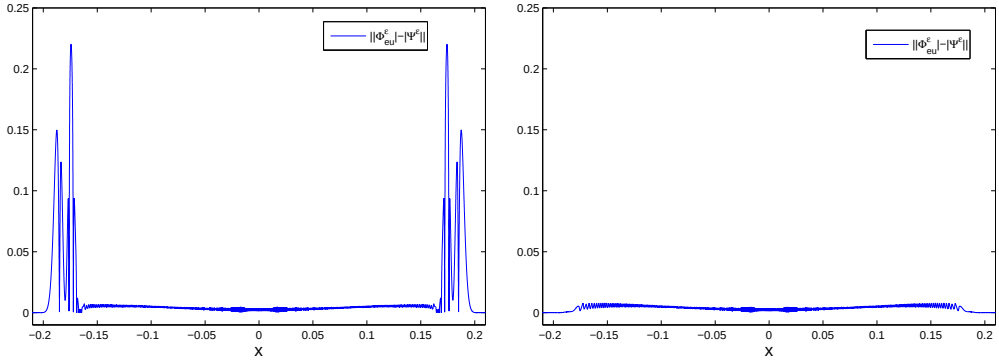

(c) Errors

Figure 6: Example 3, $\varepsilon = 1 \times 10^{-4}$. The figure shows the comparison of the wave amplitude between the Eulerian beam solution Φ^{ε}_{eu} and the Schrödinger solution Ψ^{ε} at $t = 0.5$. The Eulerian beam solution on the left is got by the summation of all the beams centered on the mesh, and the one on the right is got by the summation of the beams which better resolve the zero contour curve around caustics.

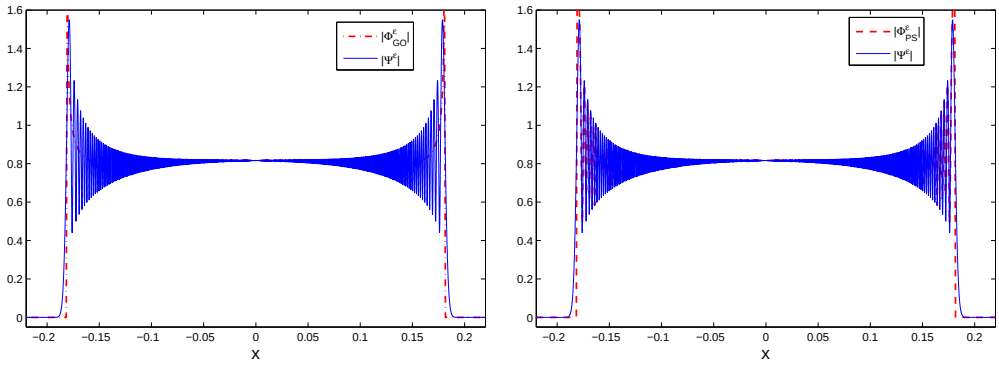

(d) Wave amplitude comparison

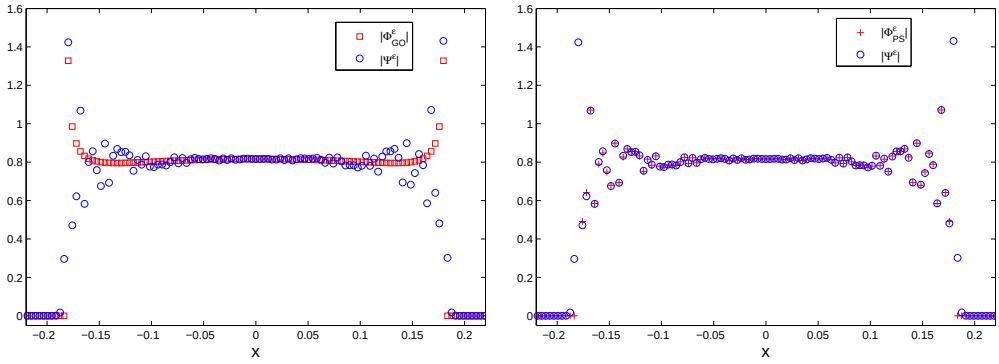

(e) Undersampled wave amplitude Comparison

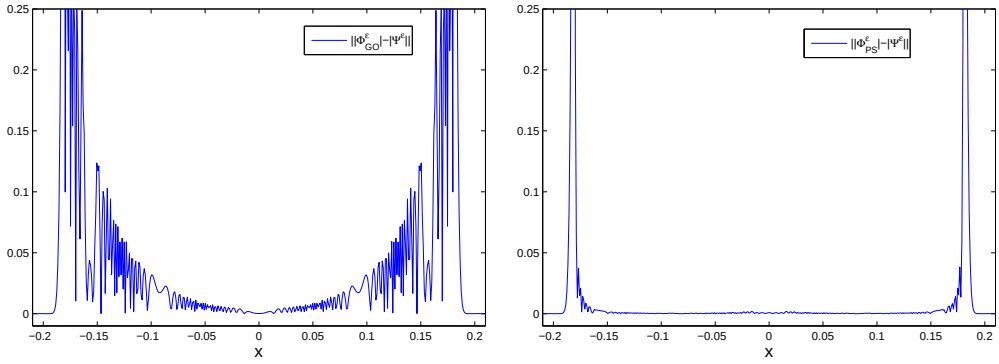

(f) Errors

Figure 6: (continued). Left: the comparison between the geometric optics approximation Φ^{ε}_{GO} and the Schrödinger solution Ψ^{ε}; right: the comparison between the geometric optics corrected with phase shift (Keller-Maslov index) Φ^{ε}_{PS} and the Schrödinger solution Ψ^{ε}.

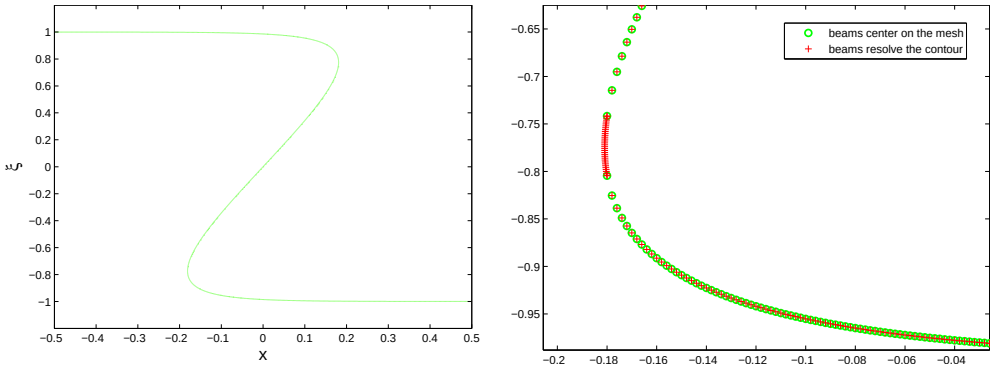

Figure 7: Example 3, t=0.5. The left figure shows the multivalued velocity; the right figure shows the beams centered on the mesh and the beams needed to resolve the zero contour around the caustic point. The former case does not resolve the caustic–around $x = -0.18$ well thus causes errors shown in Figure 6(c) (left).

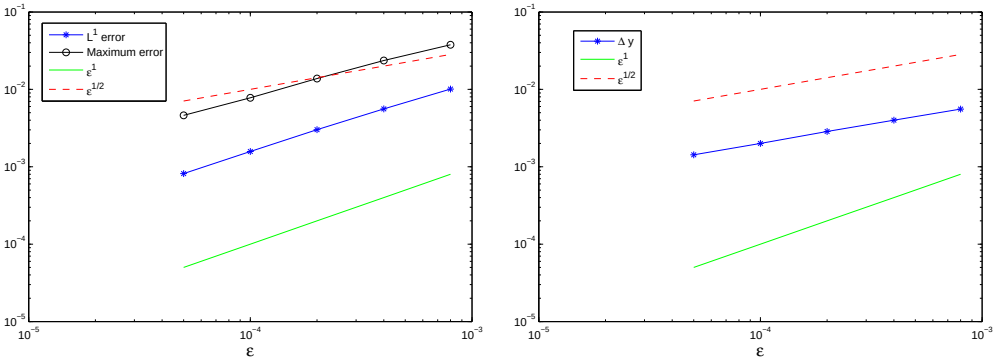

Figure 8: Example 3. Left: the convergence rate in ε of the l^1 and l^∞ errors of the wave amplitude; right: the plot of the optimal Δy for each ε.

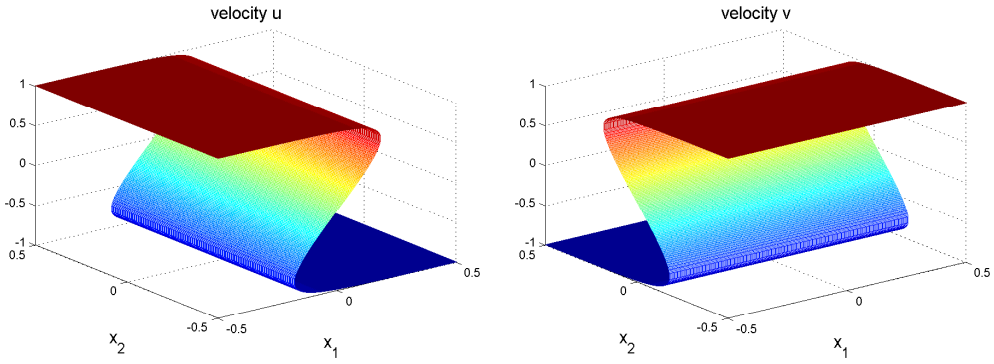

Figure 9: Example 4, the two components of the multivalued velocity at $t = 0.5$.

then the initial density and two components of the velocity are

$$\rho_0(x_1, x_2) = \exp(-50(x_1^2 + x_2^2)),$$

$$u_0(x_1, x_2) = -\tanh(5x_1), \quad v_0(x_1, x_2) = -\tanh(5x_2).$$

This is an easily-implemented two-dimensional example, since the two components are either x_1-isotropic or x_2-isotropic (see Figure 9). More complicated examples could be dealt with similarly, but one needs more sophisticated interpolation technique to get the intersection of the zero-level contours. We do not address this issue here and refer to [23] for interested readers. We use $\Delta y_1 = \Delta y_2 = \Delta\xi_1 = \Delta\xi_2 = 0.004$ for the computation of the Liouville equations (3.5) and (3.9) by the semi-Lagrangian method [19, 20]. The mesh size is $\Delta x_1 = \Delta x_2 = \dfrac{1}{65536}$ for the construction of the Eulerian beam solution (3.21). We take $\varepsilon = 0.001$ and compare the wave amplitudes of the Schrödinger solution Ψ^ε and the Eulerian beam solution Φ^ε_{eu} in Figure 10 at the time $t = 0.5$. The error between them is shown in Figure 11.

5 Conclusion

In this paper, we present the Lagrangian and Eulerian formulations of the Gaussian beam method for solving the Schrödinger equation. A new Eulerian Gaussian beam method is developed using the level set method. By using the observation (3.3), we evaluate the Hessian matrix of the phase directly from the first derivatives of the (complexified) level set function for velocity, thus avoid using an extra $2n^2$ (for n space dimension) complex-valued, inhomogeneous Liouville equations as was done in [19]. We verify the accuracy of the Gaussian beam solutions by several numerical examples which show small error around caustics. We also point out that one needs

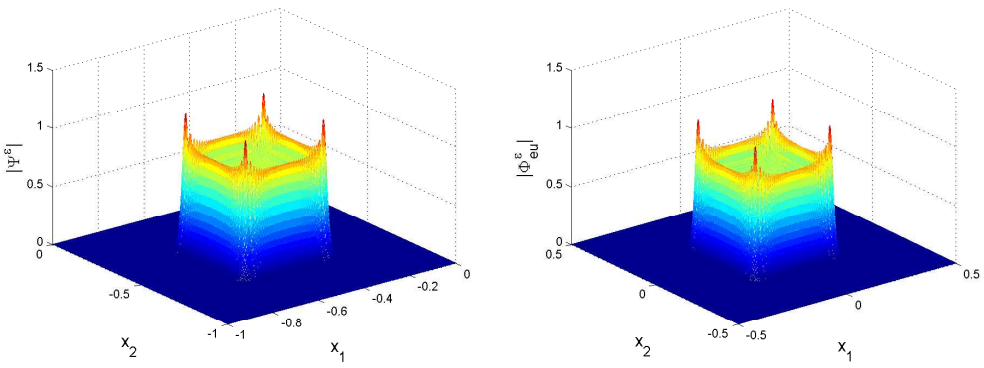

Figure 10: Example 4, the comparison of the wave amplitude between the Schrödinger solution Ψ^ε on the left and the Eulerian beams solution Φ^ε_{eu} on the right for $\varepsilon = 0.001$ and at $t = 0.5$.

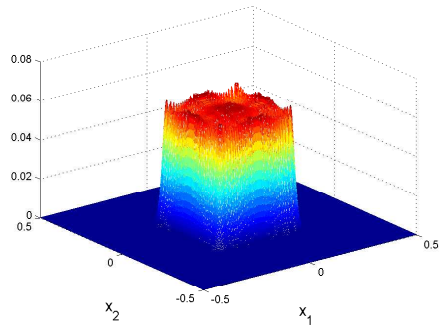

Figure 11: Example 4, the error plot of $||\Psi^\varepsilon| - |\Phi^\varepsilon_{eu}||$.

to resolve the velocity contour near caustics to obtain good approximations in the Eulerian formulation. Moreover, we give a numerical criteria for the optimal choice of the beam numbers in the Gaussian beam summation. We will extend this method to other problems in high frequency waves in the near future.

Acknowledgement

Xu Yang would like to thank Prof. Björn Engquist and Prof. Richard Tsai for the kind invitation to the workshop on Gaussian beams held in ICES, Austin, TX, which made him start to know and become interested in this subject.

Appendix

The Lagrangian summation formulation (2.28) reads as

$$\Phi^{\varepsilon}_{la}(t,\boldsymbol{x}) = \int_{\mathbb{R}^n} \left(\frac{1}{2\pi\varepsilon}\right)^{\frac{n}{2}} r_\theta(\boldsymbol{x}-\boldsymbol{y}(t,\boldsymbol{y}_0))\varphi^{\varepsilon}_{la}(t,\boldsymbol{x},\boldsymbol{y}_0)\mathrm{d}\boldsymbol{y}_0, \tag{A-1}$$

which is equivalent to

$$\Phi^{\varepsilon}_{eu}(t,\boldsymbol{x}) = \int_{\mathbb{R}^n}\int_{\mathbb{R}^n} \left(\frac{1}{2\pi\varepsilon}\right)^{\frac{n}{2}} r_\theta(\boldsymbol{x}-\boldsymbol{y})\varphi^{\varepsilon}_{eu}(t,\boldsymbol{x},\boldsymbol{y},\boldsymbol{p})\delta(\mathrm{Re}[\boldsymbol{\phi}](0,\boldsymbol{y}_0,\boldsymbol{p}_0))\mathrm{d}\boldsymbol{p}_0\mathrm{d}\boldsymbol{y}_0. \tag{A-2}$$

based on $\mathrm{Re}[\nabla_{\boldsymbol{p}_0}\boldsymbol{\phi}](0,\boldsymbol{y}_0,\boldsymbol{p}_0) = I$. Note that the integrated variables $\boldsymbol{y}_0, \boldsymbol{p}_0$ are the initial positions of $\boldsymbol{y}, \boldsymbol{p}$. Changing variables by $\boldsymbol{y}, \boldsymbol{p}$, we get

$$\Phi^{\varepsilon}_{eu}(t,\boldsymbol{x}) = \int_{\mathbb{R}^n}\int_{\mathbb{R}^n} \left(\frac{1}{2\pi\varepsilon}\right)^{\frac{n}{2}} r_\theta(\boldsymbol{x}-\boldsymbol{y})\varphi^{\varepsilon}_{eu}(t,\boldsymbol{x},\boldsymbol{y},\boldsymbol{p})\delta(\mathrm{Re}[\phi](t,\boldsymbol{y},\boldsymbol{p}))\mathrm{d}\boldsymbol{p}\mathrm{d}\boldsymbol{y}. \tag{A-3}$$

in which we need $\det J = 1$ for

$$J = \begin{pmatrix} \nabla_{\boldsymbol{y}_0}\boldsymbol{y} & \nabla_{\boldsymbol{p}_0}\boldsymbol{y} \\ \nabla_{\boldsymbol{y}_0}\boldsymbol{p} & \nabla_{\boldsymbol{p}_0}\boldsymbol{p} \end{pmatrix}.$$

First it is easy to see $\det J|_{t=0} = 1$. Moreover, we have

$$\frac{\mathrm{d}J}{\mathrm{d}t} = UJ,$$

with $U = \begin{pmatrix} 0 & I \\ -\nabla^2_{\boldsymbol{y}}V & 0 \end{pmatrix}$. This gives

$$\frac{\mathrm{d}}{\mathrm{d}t}(\det J) = \mathrm{tr}(\mathrm{adj}(J)\frac{\mathrm{d}J}{\mathrm{d}t}) = \mathrm{tr}(\mathrm{adj}(J)UJ) = \mathrm{tr}(UJ\mathrm{adj}(J)) = \det(J)\mathrm{tr}(U) = 0.$$

References

[1] W. Bao, S. Jin and P. A. Markowich, *On time-splitting spectral approximations for the Schrödinger equation in the semiclassical regime*, J. Comput. Phys. 175 (2002), no. 2, 487–524.

[2] J. D. Benamou, *Big ray tracing: Multivalued travel time field computation using viscosity solutions of the eikonal equation*, J. Comp. Phys., 128 (1996), 463-474.

[3] J. D. Benamou, *Direct computation of multivalued phase space solutions for Hamilton-Jacobi equations*, Comm. Pure Appl. Math., 52 (1999), 1443-1457.

[4] V. Cerveny, M. M. Popov and I. Psencik, *Computation of wave fields in inhomogeneous media - Gaussian beam approach*, Geophys. J. R. Astr. Soc., 70 (1982), 109-128.

[5] L.-T. Cheng, H. Liu, and S. Osher, *Computational high-frequency wave propagation using the level set method, with applications to the semiclassical limit of Schrödinger equations*, Commun. Math. Sci., 1 (2003), no. 3, 593-621.

[6] R. Courant and D. Hilbert, **Methods of Mathematical Physics**, Vol. II, Interscience Publishers, 1962.

[7] L. Dieci and T. Eirola, *Preserving monotonicity in the numerical solution of Riccati differential equations*, Numer. Math., 74 (1996), no. 1, 35-47.

[8] B. Engquist and O. Runborg, *Computational high frequency wave propagation*, Acta Numerica, 12 (2003), 181-266.

[9] B. Engquist, O. Runborg and A. K. Tornberg, *High frequency wave propagation by the segment projection method*, J. Comp. Phys., 178 (2002), 373-390.

[10] L. Gosse, *Using K-branch entropy solutions for multivalued geometric optics computations*, J. Comput. Phys., 180 (2002), no. 1, 155–182.

[11] L. Gosse, S. Jin and X. T. Li, *On two moment systems for computing multiphase semiclassical limits of the Schrödinger equation*, Math. Models Meth. Appl. Sci. , 13 (2003), no. 12, 1689-1723.

[12] N.R. Hill, *Gaussian beam migration*, Geophysics, 55 (1990), No. 11, 1416-1428.

[13] N. R. Hill, *Prestack Gaussian-beam depth migration*, Geophysics, 66 (2001), no. 4, 1240-1250.

[14] S. Jin and X. T. Li, *Multi-phase computations of the semiclassical limit of the Schrödinger equation and related problems: Whitham vs. Wigner*, Physica D, 182 (2003), 46-85.

[15] S. Jin, H. Liu, S. Osher and R. Tsai, *Computing multi-valued physical observables the semiclassical limit of the Schrödinger equations*, J. Comp. Phys., 205 (2005), 222-241.

[16] S. Jin and S. Osher, *A level set method for the computation of multivalued solutions to quasi-linear hyperbolic PDEs and Hamilton-Jacobi equations*, Commun. Math. Sci., 1 (2003), no. 3, 575-591.

[17] S. Jin and X. Yang, *Computation of the semiclassical limit of the Schrödinger equation with phase shift by a level set method*, J. Sci. Comp., to appear.

[18] S. Leung and J. Qian, *Eulerian Gaussian beams for Schrödinger equations in the semi-classical regime*, preprint.

[19] S. Leung, J. Qian and R. Burridge, *Eulerian Gaussian beams for high-frequency wave propagation*, Geophysics, 72 (2007), no. 5, 61-76.

[20] S. Leung, J. Qian and S. Osher, *A level set method for three dimensional paraxial geometrical optics with multiple sources*, Commun. Math. Sci., 2 (2004), no. 4, 643-672.

[21] P. A. Markowich, P. Pietra and C. Pohl, *Numerical approximation of quadratic obaservables of Schrödinger-type equations in the semiclassical limit*, Numer. Math., 81 (1999), 595-630.

[22] P. A. Markowich, P. Pietra, C. Pohl and H. P. Stimming, *A wigner-measure analysis of the Dufort-Frankel scheme for the Schrödinger equation*, SIAM J. Num. Anal., 40 (2002), 1281-1310.

[23] C. Min, *Simplicial isosurfacing in arbitrary dimension and codimension*, J. Comp. Phys., 190 (2003), no. 1, 295–310.

[24] M. Motamed and O. Runborg, *Taylor expansion errors in Gaussian beam summation*, preprint.

[25] M. Motamed and O. Runborg, *A wave front-based Gaussian beam method for computing high frequency waves*, preprint.

[26] S. Osher, L.-T. Cheng, M. Kang, H. Shim and Y.-H. Tsai, *Geometric optics in a phase-space-based level set and Eulerian framework*, J. Comput. Phys., 179 (2002), no. 2, 622-648.

[27] D. Peng, B. Merriman, S. Osher, H. Zhao and M. Kang, *A PDE based fast local level set method*, J. Comput. Phys., 155 (1999), 410-438.

[28] M. M. Popov, *A new method of computation of wave fields using gaussian beams*, Wave Motion, 4 (1982), 85-97.

[29] J. Ralston, *Gaussian beams and the propagation of singularities*, Studies in PDEs, MAA stud. Math., 23 (1982), 206-248.

[30] N. M. Tanushev, *Superpositions and higher order Gaussian beams*, Commun. Math. Sci., 6 (2008), no. 2, 449-475.

[31] N.M. Tanushev, J.L. Qian and J. Ralston, *Mountain Waves and Gaussian Beams*, SIAM Multiscale Modeling and Simulation, 6 (2007), 688-709.

[32] G. B. Whitham, **Linear and Nonlinear Waves**, Wiley, New York, 1974.